Ultrafine Membrane Compartments for Molecular Diffusion as Revealed by Single Molecule Techniques

Kotono Murase,* Takahiro Fujiwara,* Yasuhiro Umemura,† Kenichi Suzuki,* Ryota Iino,* Hidetoshi Yamashita,† Mihoko Saito,† Hideji Murakoshi,† Ken Ritchie,*† and Akihiro Kusumi*†

*Kusumi Membrane Organizer Project, Exploratory Research for Advanced Technology Organization (ERATO/SORST), Japan Science and Technology Agency, Nagoya, Japan and †Department of Biological Science and Institute for Advanced Research, Nagoya University, Nagoya, Japan

ABSTRACT Plasma membrane compartments, delimited by transmembrane proteins anchored to the membrane skeleton (anchored-protein picket model), would provide the membrane with fundamental mosaicism because they would affect the movement of practically all molecules incorporated in the cell membrane. Understanding such basic compartmentalized structures of the cell membrane is critical for further studies of a variety of membrane functions. Here, using both high temporal-resolution single particle tracking and single fluorescent molecule video imaging of an unsaturated phospholipid, DOPE, we found that plasma membrane compartments generally exist in various cell types, including CHO, HEPA-OVA, PtK2, FRSK, HEK293, HeLa, T24 (ECV304), and NRK cells. The compartment size varies from 30 to 230 nm, whereas the average hop rate of DOPE crossing the boundaries between two adjacent compartments ranges between 1 and 17 ms. The probability of passing a compartment barrier when DOPE is already at the boundary is also cell-type dependent, with an overall variation by a factor of ~7. These results strongly indicate the necessity for the paradigm shift of the concept on the plasma membrane: from the two-dimensional fluid continuum model to the compartmentalized membrane model in which its constituent molecules undergo hop diffusion over the compartments.

INTRODUCTION

One of the most important structural characteristics of the cell membrane is that it behaves like a two-dimensional liquid, and its constituent molecules, i.e., membrane proteins and lipids, rapidly move about in the membrane plane. However, even phospholipids do not undergo free diffusion in the cellular plasma membrane. The diffusion rates in the cell membrane are reduced by a factor of 10–100, as compared to those in artificial membranes (see Table 1). The mechanism that is responsible for such slowing has puzzled membrane biologists for the last 25 years.

Fujiwara et al. (2002) addressed this issue using both single fluorescent molecule video imaging (SFVI) (for reviews see Schütz et al., 2000; Iino and Kusumi, 2001) and single particle tracking (SPT) (for reviews see Kusumi and Sako, 1996; Saxton and Jacobson, 1997) with time resolutions of up to 25 μs. They found that the unsaturated phospholipid, 1,2-dioleoyl-*sn*-glycero-3-phosphoethanolamine (DOPE), in the outer leaflet of the plasma membrane of NRK cells, is confined within compartments of 230 nm on average, on short timescales (11 ms on average). On longer timescales, DOPE undergoes hop movements among adjacent compartments, as observed previously with transmembrane proteins by Sako and Kusumi (1994). Fujiwara et al. (2002) found that the membrane skeleton is primarily responsible for such temporal confinement, and proposed the ''anchored membrane-protein picket model'', in which various transmembrane proteins anchored to the actin-based membrane skeleton effectively act as rows of pickets along the membrane skeleton fence, due to the effects of steric hindrance and circumferential slowing (Fujiwara et al., 2002). Circumferential slowing is the collective term for hydrodynamic friction (in terms of hydrodynamic theory, Bussell et al., 1995; Dodd et al., 1995) and increased packing (in terms of free-volume theory, Sperotto and Mouritsen, 1991; Almeida et al., 1992), and is highly enhanced near immobile transmembrane proteins.

The diffusion rates of lipids vary greatly from cell to cell, with an overall variation by a factor of ~15 (see Table 1). FRSK cells have displayed one of the slowest diffusion rates studied thus far (because the data obtained in this research have been added to the table, the diffusion coefficient of lipid in FRSK cells does not appear to be particularly slow; however, when this work was initiated, it was one of the smallest in the literature). In this research, we examined the mechanism for slowing the lipid diffusion in FRSK cells (as well as CHO, HEPA-OVA, PtK2, HEK293, HeLa, and T24 (ECV304, a subclone of T24) cells), and investigated how this slower diffusion rate is induced in FRSK cells.

Even in FRSK cells, DOPE was found to undergo hop diffusion, in a manner dependent on the membrane skeleton, but not on the cholesterol concentration, the extracellular matrix, and the extracellular domains of membrane proteins, consistent with the anchored-protein picket model. However, compartment sizes as small as 30–40 nm were found in

Submitted October 8, 2003, and accepted for publication February 27, 2004.

Address reprint requests to Akihiro Kusumi, Ph.D., Dept. of Biological Science, Nagoya University, Nagoya 464-8602, Japan. Tel.: 81-52-789-2969; Fax: 81-52-789-2968; E-mail: akusumi@bio.nagoya-u.ac.jp.

Ryota Iino's present address is Yoshida ATP System Project, ERATO, JST, Nagatsuda 5800-3, Midori-ku, Yokohama 226-0026, Japan.

0006-3495/04/06/4075/19 $2.00

doi: 10.1529/biophysj.103.035717

FRSK, CHO, HEPA-OVA, and PtK2 cells (~70 nm in HEK293 and HeLa cells, 110 nm in T24 cells, and 230 nm in NRK cells), which are smaller by a factor of ~7 in diameter (or a factor of ~50 in area) than those previously found in NRK cells.

To obtain the correct hop rates of membrane molecules, the following method has been used extensively in this study (Fujiwara et al., 2002): the macroscopic diffusion coefficient over many compartments was obtained using SFVI, and the compartment size was obtained by high temporal/spatial-resolution single-particle tracking using 40-nm colloidal-gold probes. Since fluorescent probes, which are much smaller than colloidal-gold probes, are much less likely to interact with other molecules, and since they intrinsically represent single molecules, unlike gold probes, with which one must always carefully consider the level of crosslinking when interpreting the data, SFVI tends to provide much more reliable data on the macroscopic diffusion coefficient. However, the time resolution obtained by SFVI is limited to a millisecond at best, and this cannot be accomplished without severely sacrificing the observation durations (due to photobleaching by the employment of high excitation light intensity; Schütz et al., 2000). Our past experience indicated that to identify membrane compartments clearly by statistical analyses as well as by eye, one should observe a single molecule's trajectory for a sufficiently long period to include more than a few hops *and* with a time resolution high enough to have at least 40 points (on average) within a compartment. If the residency time within a compartment is short (i.e., the hop rate is high), e.g., from one to several hundred milliseconds, then such conditions cannot be fulfilled with single fluorescent molecule observations, but can be easily satisfied by high-speed SPT with gold probes (Fujiwara et al., 2002).

If the gold probe induces (even low levels of) crosslinking, then it would affect the hop rate strongly (this is already a strong indication that the plasma membrane should not be thought as a two-dimensional fluid continuum), but the observed compartment size only slightly. Therefore, the hop rate can be calculated quite accurately by using the macroscopic diffusion coefficient of a fluorescently-labeled lipid (DOPE) and the compartment size determined by SPT with gold-probe-labeled DOPE.

Hop rates measured for DOPE are as fast as once every ~1–2 ms in FRSK, CHO, HEPA-OVA, and PtK2 cells (~3 ms for HEK293 cells, ~5 ms for HeLa cells, and ~10–20 ms for T24 and NRK cells) on average. Although the residency time is very short for DOPE, it was greatly prolonged upon the crosslinking of DOPE. This suggests that when receptor molecules are liganded and clustered to form signaling complexes, they will be instantaneously arrested in the membrane skeleton mesh (oligomerization-induced trapping model; Iino et al., 2001). Further, if larger and stabilized rafts were induced upon clustering of GPI-anchored or other raft-preferring receptor molecules, the results presented here indicate they too have to be trapped in the compartment where the stabilized rafts are formed. Therefore, the ''pickets'' and ''fences'' made of the membrane skeleton and the anchored transmembrane proteins provide the cell with a mechanism for preserving the spatial information of signal transduction in the membrane.

One of the most important questions addressed in this research is: How universal is the compartmentalized structure of the membrane that even works for phospholipids? We started out from very detailed examinations of the DOPE diffusion in FRSK cells, where the DOPE diffusion is substantially slower than that reported previously (Table 1). Then we further proceeded 1), to examine whether hop diffusion is found in other cell types and 2), to obtain the compartment sizes and the hop rates if hop diffusion is found in those cells. SFVI of fluorescently-labeled DOPE and high-speed SPT of gold-particle-tagged DOPE have been carried out for all of the eight cells examined thus far, suggesting that the plasma membrane compartmentalization and the hop diffusion of membrane molecules occur universally among mammalian cells. The compartmentalization of the plasma membrane and hop diffusion of lipid molecules over these compartments were found in all of the eight cells examined here. This strongly indicates the necessity for the paradigm shift of our view on the plasma membrane, from the two-dimensional fluid continuum model to the compartmentalized membrane model in which its constituent molecules undergo hop diffusion over these compartments.

MATERIALS AND METHODS

Cell culture

Fetal rat skin keratinocytes (FRSK, a cell line) were grown in Eagle's minimal essential medium (MEM) supplemented with 10% fetal bovine serum. Cells used for the experiment were cultured on 18×18-mm coverslips (IWAKI, Chiba, Japan) for high-speed video imaging and cell staining for 2 days after plating, or on 12-mm ϕ glass-bottom dishes (IWAKI) for single fluorescence molecule video imaging for one day after plating (FRSK cells grow faster in the glass-bottom dishes). All other cells were observed on the second day after inoculation in either type of dish.

Synthesis of Cy3-DOPE

DOPE (Avanti Polar Lipids, Alabaster, AL, 6 μmol), dissolved in 500 μl of $CHCl_3$ containing 20 μl dry $(C_2H_5)_3N$, was added to a solution of 3 μmol Cy3.29-succinimidyl ester (monoreactive, Amersham-Pharmacia, Tokyo, Japan) in 50 μl dry dimethylformamide. The solution was stirred under a nitrogen atmosphere at room temperature for 2 h. Next, silica-gel thin layer chromatography (TLC) ($CHCl_3$: MeOH: H_2O = 2:1:1 vol/vol) was used to identify the presence of a new spot ($R_f = 0.6$) and then to isolate the product: after the reaction mixture was evaporated to dryness, the crude product was dissolved in a mixture of $CHCl_3$/MeOH/H_2O (7:3:0.4 vol/vol), applied to a preparative TLC plate, and developed in the same solvent mixture, and then the Cy3-DOPE spot was scraped off from the TLC plate. For the synthesis of FITC-DOPE, 20 μmol fluorescein-5-isothiocyanate (isomer I from Molecular Probes, Eugene, OR) was added to 20 μmol of DOPE in 2 ml $CHCl_3$ containing 2 μl dry $(C_2H_5)_3N$. The solution was stirred under a nitrogen atmosphere at room temperature for 2 h. A new spot exhibiting the

TABLE 1 Diffusion coefficients for lipids in artificial and cell membranes

Probe*	Membrane type†	Method‡	Mobile fraction (%)	D mean (±SD; $\mu m^2/s$)	Time-window for D (ms)	Temp. (°C)	Reference
Artificial membranes							
TRITC(Cy5)-DPPE	POPE:POPC = 7:3	SFD	100	20.6 (±0.9)	40	23	Sonnleitner et al. (1999)
EYPC	100% EYPC	NMR	?	5 (±2)	~100	35	Lindblom et al. (1981)
NBD-DPPE	100% POPC	FRAP	98	13 (±1.2)	500§	23	Ladha et al. (1996)
NBD-PE¶	100% DMPC	FRAP	~100	7.6 (±0.3)	2000§	30	Chang et al. (1981)
NBD-PE¶	Erythrocyte total lipid	FRAP	~100	3.4 (±0.3)	4000§	30	Chang et al. (1981)
NBD-eggPE	100% DMPC	FRAPP	?	5 (±0.3)	~3000‖	26	Smith et al. (1980)
NBD-DMPE	100% DMPC	FRAPP	?	4.3 (±0.2)	~3000‖	32	Smith et al. (1980)
Gold-DOPE	eggPC:PS:DOPE = 500:50:1	SPT	100	9.4 (±3.7)	100	37	Fujiwara et al. (2002)
Cellular plasma membranes							
Cy5-DMPE	HASM	SFD	100	0.6 (±0.04)	12	RT	Schütz et al. (2000)
Cy3-DOPE	NRK	SFVI	100**	0.41 (±0.13)††	100	37	Fujiwara et al. (2002)
Cy3-DOPE	CHO-B1	SFVI	100**	0.30 (±0.23)††	100	37	This work
Cy3-DOPE	T24	SFVI	100**	0.22 (±0.14)††	100	37	This work
Cy3-DOPE	FRSK	SFVI	100**	0.27 (±0.20)††	100	37	This work
Cy3-DOPE	HEK293	SFVI	100**	0.41 (±0.18)††	100	37	This work
Cy3-DOPE	HEPA-OVA	SFVI	100**	0.37 (±0.43)††	100	37	This work
Cy3-DOPE	HeLa	SFVI	100**	0.31 (±0.31)††	100	37	This work
Cy3-DOPE	Melanocytes	SFVI	100**	0.40 (±0.28)††	100	37	This work
Cy3-DOPE	PtK2	SFVI	100**	0.53 (±0.30)††	100	37	This work
F18	Bull sperm: acrosome	FRAP	94	2.93 (±0.15)	~200§	20	Ladha et al. (1997)
F18	Bull sperm: principal piece	FRAP	90	1.18 (±0.26)	~400§	20	Ladha et al. (1997)
NBD-PC¶	3T3-B	FRAP	54	0.19 (±0.11)	~10,000‡‡	?	Swaisgood and Schindler (1989)
NBD-PC¶	KMSV-3T3	FRAP	70	0.35 (±0.23)	~10,000‡‡	?	Swaisgood and Schindler (1989)
FITC-DPPE	C3H (lamella)	FRAP	69	0.54 (±0.27)	~350–700§§	RT¶¶	Lee et al. (1993)
FITC-DPPE	PtK1 (lamella)	FRAP	71	0.63 (±0.13)	~350–700§§	RT¶¶	Lee et al. (1993)
FITC-DPPE	Fish scale fibroblast	FRAP	74	0.95 (±0.17)	~350–700§§	RT¶¶	Lee et al. (1993)

*TRITC-DPPE, *n*-(6-tetramethylrhodaminethiocarbamoyl)-1,2-dihexadecanoyl-*sn*-glycero-3-phosphoethanolamine; EYPC, egg yolk phosphatidylcholine; NBD, *n*- (4-nitrobenzo-2-oxa-1,3-diazole); DMPE, 1,2-dimyristoyl-*sn*-glycero-3-phosphoethanolamine; FITC, fluorescein isothiocyanate; DOPE, 1,2-dioleoyl-*sn*-glycero-3-phosphoethanolamine; F18, 5-(*n*-octa-decanoyl)aminofluorescein.

†POPE, 1-palmitoyl-2-oleoyl-*sn*-glycero-3-phosphoethanolamine; POPC, 1-palmitoyl-2-oleoyl-*sn*-glycero-3-phosphocholine; DMPC, 1, 2-dimyristoyl-*sn*-glycero-3-phosphocholine; PS, bovine brain phosphatidylserine; NRK, normal rat kidney fibroblasts; HASM, human coronary artery smooth muscle; T24, human epithelial carcinoma cells; FRSK, fetal rat skin keratinocyte; PtK2, rat kangaroo normal kidney; CHO-B1, CHO-K1 cells (Chinese hamster ovary) transfected with murine Fcγ receptor type B1, called CHO-B1 (Miettinen et al., 1989; 1992); HEK293, human embryonic kidney; HEPA-OVA, mouse hepatoma cells; HeLa, Homo sapiens cervix; melanocytes, murine amelanotic melan-c melanocytes; 3T3-B, BALB/c 3T3 fibroblasts; KMSV-3T3, Kirsten murine sarcoma virus-transformed 3T3-B fibroblasts; C3H, mouse embryo fibroblasts; PtK1, rat kangaroo normal kidney.

‡SFD, single fluorescence molecule detection (epifluorescence); NMR, nuclear magnetic resonance; FRAP, fluorescence recovery after photobleaching; FRAPP, fluorescence recovery after pattern photobleaching; SPT, single particle tracking; SFVI, single fluorescence molecule video imaging.

§The time required for half of the observed fluorescence recovery to occur, read off from the published recovery curves.

¶Unknown acyl chains.

‖The half-time of the total observation period after pattern photobleaching.

**Fluctuation (noise) of the coordinates determined for Cy3-DOPE molecules attached on the coverslip (immobile control) gave the nominal diffusion coefficients in the range between 3.0×10^{-4} and 5.9×10^{-3} $\mu m^2/s$. Meanwhile, all fluorescent spots observed in these studies exhibited diffusion coefficients $>5.9 \times 10^{-3}$ $\mu m^2/s$, and thus it was concluded that the mobile fraction was 100%.

††These SDs include, in addition to the experimental error, the true variations in the diffusion coefficient for individual molecules. The distribution in FRSK cells is given in Fig. 2.

‡‡The time required for half of the observed fluorescence recovery to occur, read off from Koppel (1979).

§§The time required for half of the observed fluorescence recovery to occur (K. Jacobson, personal communication).

¶¶K. Jacobson, personal communication.

production of FITC-DOPE ($R_f = 0.6$) was identified by TLC ($CHCl_3$/MeOH = 4:1). FITC-DOPE was purified as follows: After the reaction mixture was evaporated to dryness, the crude product was dissolved in a mixture of $CHCl_3$/MeOH = 4:1 (v/v) and applied to a 10-g silica gel column C-300 HG from Wako (Osaka, Japan), and then eluted with a $CHCl_3$/MeOH = 4:1 (v/v) solvent mixture. The fractions with equal R_f values were combined and evaporated to dryness.

Preparation of colloidal-gold probes

The minimal protecting amount (MPA) of anti-fluorescein antibodies' Fab fragments (Molecular Probes), which is defined as the minimum concentration of the protein needed to stabilize colloidal gold in suspension, was determined to be 2.5 μg/ml, using methods described previously (De Mey, 1983; Leunissen and De Mey, 1989). Colloidal-gold probes created

with attached to the MPA of Fab were prepared by mixing 50 μl of 25 μg/ml anti-fluorescein Fab in 2 mM phosphate buffer (pH 7.2) and a 500 μl suspension of colloidal gold (pH 7.4) on a slowly tumbling shaker for 1 h at room temperature. The gold probe was further stabilized with 0.05% Carbowax 20M (Sigma, St. Louis, MO). After three washes by sedimentation and resuspension in 0.05% Carbowax 20M in 20 mM phosphate buffer (pH 7.0), the gold probe was resuspended in Eagle's minimal essential medium (MEM) containing 2 mM PIPES (without $NaHCO_3$) and 10% fetal bovine serum, sterilized by filtration with a 0.22-μm filter (Millipore, Bedford, MA), and then used within 12 h.

Single fluorophore video imaging of Cy3-DOPE and single particle tracking of Gold-DOPE

For SFVI of Cy3-DOPE, first Cy3-DOPE in methanol (20 μg/ml) was added to HBSS buffered with 2 mM PIPES at pH 7.2 with vigorous vortexing (100 ng/ml final concentration), and then this solution was then added to the cells cultured on a glass-bottom dish at 37°C (final concentration 10 ng/ml). Individual Cy3-DOPE molecules were observed in the apical cell membrane (side of the membrane facing the medium) at the video rate, using a homebuilt objective lens-type total internal reflection fluorescence microscope (Iino et al., 2001). Briefly, a 532-nm laser beam (the second harmonic of the Nd:YAG laser beam, Model 4501-050, Uniphase, San Jose, CA) was attenuated with neutral density filters, circularly polarized, and then steered into the edge of a high numerical aperture (NA) objective lens (PlanApo100 $\times$, NA = 1.4 or 1.45, Olympus, Tokyo, Japan) with a focus at the back-focal plane of the objective lens on an Olympus inverted microscope (IX-70).

For SPT of Gold-DOPE, after FITC-DOPE was incorporated in the cell membrane by the addition of 2 μg/ml (final concentration) of FITC-DOPE, gold probes conjugated with anti-fluorescein antibodies' Fab fragments were applied to cells cultured on 18 $\times$ 18-mm coverslips. For observation with improved temporal resolutions, a digital high-speed camera with a C-MOS sensor was used (FASTCAM-Ultima, PHOTRON, Tokyo, Japan; Tomishige et al., 1998, Fujiwara et al., 2002). For high-speed video microscopy, bright-field optical microscopy rather than Nomarski microscopy was employed, and the green interference filter was removed to increase the light intensity on the photodetector plane, greatly enhancing the signal/noise ratio in the image. The sequence of images was replayed at the video rate with analog and digital enhancements by an image processor (DVS-3000, Hamamatsu Photonics, Hamamatsu, Japan), and recorded on a digital video tape recorder (DSR-20, Sony, Tokyo, Japan).

Positions of single gold particles or single fluorescent molecules were determined from each image, and the mean-squared displacement versus time (MSD-t) plots were obtained as described previously (Kusumi et al., 1993). From video-rate recordings, the diffusion coefficients in a 100-ms time-window (D_{100ms}) were obtained, which is the same as D_{2-4} in Kusumi et al. (1993).

In SPT recordings at time resolutions of 110 or 25 μs, typically, recordings for 278 or 61.7 ms (2500 frames), respectively, were carried out for at least 35 particles. Almost all of the MSD-t curves showed a rapid rise followed by a leveling off. The MSD-t plot was fitted to a theoretical curve representing hop diffusion (Powles et al., 1992). For successful curve fitting, the duration for the fit must be sufficiently long to reflect the macroscopic diffusion, but should not be overly long so that the behavior near time 0 and the largest curvature in the transition region between the short-term simple Brownian diffusion and the long-range hop movements over the compartments are properly taken into account. Generally, 8.89 and 6.17 ms for 110- or 25-μs resolutions, respectively, turned out to be useful. The fit parameters included L, the compartment size, and D_{MACRO}, the macroscopic diffusion coefficient over the membrane compartments, and D_{micro} (typically $\approx D_{100\mu s}$); both represent the diffusion coefficients within a compartment when the compartment size is sufficiently large, $\approx$800 nm or greater; when the compartments are smaller, these values are artificially reduced because the averaging of the image of gold particles over the frame time—even 25 μs—makes their movement appear smaller as the compartment boundaries more frequently bounce off the molecule (see Results). The residency time, τ, was calculated from L and D_{MACRO}: $\tau = L^2/4D_{MACRO}$. $D_{100\mu s}$ (Table 2, Fig. 8) and D_{100ms} (Table 3, Table 6, and Fig. 2) were determined by fitting the MSD-t plots between the second and fourth points using a straight line (which is the same as D_{2-4} in Kusumi et al., 1993) for the data obtained at 33-ms and 25-μs resolutions, respectively.

To estimate the accuracy of the position determination, and to evaluate the slowest diffusion coefficient that can be measured at a 25-μs resolution by the present instrument, gold particles (40-nm ϕ) were observed after their binding to 1), a poly-L-lysine-coated coverslip, followed by impregnation in a 10% polyacrylamide gel at 25°C (Kusumi et al., 1993) or 2), fluorescein-DOPE preincorporated in large, unilamellar vesicles of L-α-dipalmitoylphosphatidylcholine in the gel phase at 25°C. The trajectories of these immobilized particles were obtained for at least eight particles, each 120-ms (5000 frames)-long, and the MSD-t curves were calculated over 6.17 and 22 ms and fitted as described above. All the MSD-t curves for individual particles were averaged, and the fit was carried out as described above. Standard deviations for the position determination were also evaluated to be 19 and 13 nm for gold particles on the coverslip and the DPPC membrane, respectively (Table 2).

The results of these measurements are summarized in Table 2. The mean value of the diffusion coefficients for Gold-DOPE on FRSK cells is greater than those on the coverslip or the DPPC bilayer in the gel phase by a factor of >30 in every time-window, indicating that the background noise does not make significant contributions to the diffusion coefficients of Gold-DOPE determined here. These noise factors will become important when the measured diffusion coefficients in the cell are smaller, or when the determination of the immobile fraction is desired.

Modulation of the actin cytoskeleton, partial cholesterol depletion, and membrane bleb formation

FRSK cells were incubated in the MEM medium containing either 13 μM cytochalasin D or 0.5 μM jasplakinolide (gifts from Dr. G. Marriott, University of Wisconsin-Madison) on the microscope stage at 37°C for

TABLE 2 The accuracy of the position determination for immobile gold particles and the lower limit diffusion coefficients that can be determined by this microscope-fast camera station at a time resolution of 25 μs (see Materials and Methods for details of the experimental protocols)

Substrate	$D_{100\mu s}$ ($\mu m^2/s$)*	D_{MACRO} ($\mu m^2/s$)*	D_{22ms} ($\mu m^2/s$)*†	Position accuracy (SD, nm)‡	n§
Coverslip	0.021	0.00043	0.00088	19	11
DPPC bilayer (gel phase, 25°C)	0.015	0.00078	0.00035	13	8
FRSK cells (37°C)	0.62	0.053	0.051	—	35

*For the definition of these diffusion coefficients, see Materials and Methods. Note that, in the evaluations of the diffusion coefficients here, MSD-t curves (6.17-ms long) for individual particles were first ensemble-averaged and then fitted. $D_{100\mu s}$ was determined by fitting the MSD-t plots between the second and fourth points using a straight line. D_{MACRO} was determined based on the theory of hop diffusion by Powles et al. (1992).

†For the evaluation of the nominal diffusion coefficients in a 22-ms window, 120-ms trajectories (5000 total frames) were obtained for at least eight particles, and the MSD-t plots over 22 ms were determined. After averaging over all the particles, the hop-diffusion fit based on Powles et al. (1992) was carried out and its D_{MACRO} is listed as D_{22ms}.

‡The standard deviation of the position determination.

§Number of observed particles.

TABLE 3 D_{100ms}, D_{3s}, hop rate, and residency time for Cy3-DOPE and Gold-DOPE evaluated in the membrane of FRSK cells

	D_{100ms} ($\mu m^2/s$)*		D_{3s} ($\mu m^2/s$)*				
Probe	Median	Mean ± SD	Median	Mean ± SD	Hop rate† (s^{-1})	Residency time (ms)†	n‡
Cy3-DOPE	0.19	0.27 ± 0.20	0.15	0.18 ± 0.19	440	2.3	29 (13)
Gold-DOPE	0.044	0.086 ± 0.12	0.028	0.055 ± 0.076	100	9.8	47 (37)

For D_{100ms} estimates, trajectories of 0.94–16 s long (typically ~4 s) for cy3-DOPE and 1.5–14 s long (typically ~10 s) for Gold-DOPE were collected, and their MSD-t plots were linearly fitted between the second and the fourth points (the same as D_{2-4} in Kusumi et al., 1993). For D_{3s} evaluations, trajectories longer than 3 s were collected, and their MSD-t plots were linearly fitted between 66 ms and 3 s.

*D_{100ms} and D_{3s} were observed at a 33-ms resolution (video rate). The SDs include, in addition to the experimental error, the true variations in the diffusion coefficient for individual particles. The distributions for D_{100ms} are shown in Fig. 2.

†The hop rates for Gold-DOPE and Cy3-DOPE were calculated using D_{100ms} (median), obtained by SPT of Gold-DOPE and SFVI of Cy3-DOPE (as shown in this table) and the median compartment size determined by SPT (25-μs resolution) of Gold-DOPE (41 nm), based on the relationship: $\tau = L^2/4D_{100ms}$ ($[0.041]^2/4/0.19$).

‡The numbers of observed particles for D_{100ms}. Those for D_{3s} are indicated in parentheses.

5 min. Microscopic observations were completed within 15 min after the addition of drugs.

For partial cholesterol removal, cells were incubated at 37°C for 20 min in the presence of 4 mM MβCD (Sigma) in MEM containing LDL-free FBS (Goldstein et al., 1983). To make the membrane blebs on the cell surface, cells were treated with 0.5 mM 2-methyl-1,4-naphthoquinone (menadione) in HBSS buffered with 2 mM PIPES (pH 7.4) at 37°C for 60 min (Malorni et al., 1991; Fujiwara et al., 2002).

Removal of the extracellular matrix and extracellular domains of membrane proteins on the cell surface

To remove the extracellular matrix and extracellular domains of membrane proteins from the surface, the FRSK cells were treated with 5, 10, or 25 μg/ml trypsin (Difco, Kansas City, MO) at 37°C for 10 min. To monitor the extent of cleavage, the extracellular surface proteins were first tagged with sulfosuccinimidyl biotin (Sigma), and were visualized by fluorescein-streptavidin (Molecular Probes) before and after trypsin treatment. Chondroitin sulfate glycosaminoglycan was detected by an indirect immunofluorescence method, using mouse anti-chondroitin sulfate IgM (Seikagaku, Tokyo, Japan) and TRITC-conjugated goat anti-mouse IgM (ICN, Costa Mesa, CA). Epifluorescence images of cells were quantitated by the MetaView software (Universal Imaging, Downingtown, PA).

RESULTS

DOPE undergoes slow, apparently simple Brownian diffusion in the plasma membrane of FRSK cells at a time resolution of 33 ms

All experiments were carried out at 37°C unless otherwise specified. To track the movement of individual phospholipid molecules in the cell membrane, DOPE molecules tagged with Cy3 in the headgroup region were incorporated in the cell membrane of FRSK cells, and then individual Cy3-DOPE molecules were observed under an objective-lens-type total internal reflection fluorescence microscope at video rate (33-ms resolution). The Cy3-DOPE thus observed was confirmed to be individual molecules by the single-step photobleaching and the single-peak distribution of its fluorescence intensity (data not shown), as described previously (Iino et al., 2001; Fujiwara et al., 2002). Therefore, this method is referred to as SFVI (see Introduction). A typical trajectory of a Cy3-DOPE molecule, recorded at a 33-ms resolution for a period of 3.3 s, is shown in Fig. 1 *a*.

The mean values of the diffusion coefficients in a 100-ms time-window (D_{100ms}, which is the same as D_{2-4} in Kusumi et al., 1993) and in a 3-s time-window (D_{3s}, determined by a linear fit between 66 ms and 3 s) were 0.19 $\mu m^2/s$ and 0.15 $\mu m^2/s$ (median), respectively (see Fig. 2 *A*, *top*). These values are smaller than those of lipid analogs in liposomes and reconstituted membranes, by a factor as large as ~50 (see Table I in Fujiwara et al., 2002).

Crosslinking effects of gold probes and optimization of gold-particle labeling

Such a great reduction in the diffusion coefficient in the cell membrane from the artificial membranes suggests the presence of mechanisms for restricting lipid movement in the FRSK cell membrane that are not resolvable at a 33-ms resolution. Since achieving higher time resolutions in single fluorophore observations is difficult due to the problem of low signal/noise ratios, we employed single particle tracking (SPT) by binding 40 nm-ϕ colloidal-gold probes to fluorescein-DOPE molecules preincorporated in the cell membrane. Note that the fluorescein moiety is not used as a fluorescent probe, but as a tag to anchor the gold probes on DOPE via the anti-fluorescein Fab.

Conditions for labeling DOPE with gold probes were optimized by adjusting the concentration of fluorescein-DOPE preincubated with the cells and the amount of anti-fluorescein Fab fragments conjugated with the gold probes (see Materials and Methods). Thus, the effect of crosslinking by the gold probes was minimized, while sufficient specificity for their binding to the cell surface was maintained. Reducing the Fab concentration mixed with gold probes increased the diffusion rate of the gold-DOPE complex determined at video rate (D_{100ms}), which reached a plateau value of 0.044 $\mu m^2/s$ (median) at 2.5 μg/ml of Fab. At this concentration, the ratio of particles bound specifically versus nonspecifically (using 40 nm-ϕ colloidal-gold probes not coated with Fab fragments) was 5:1.

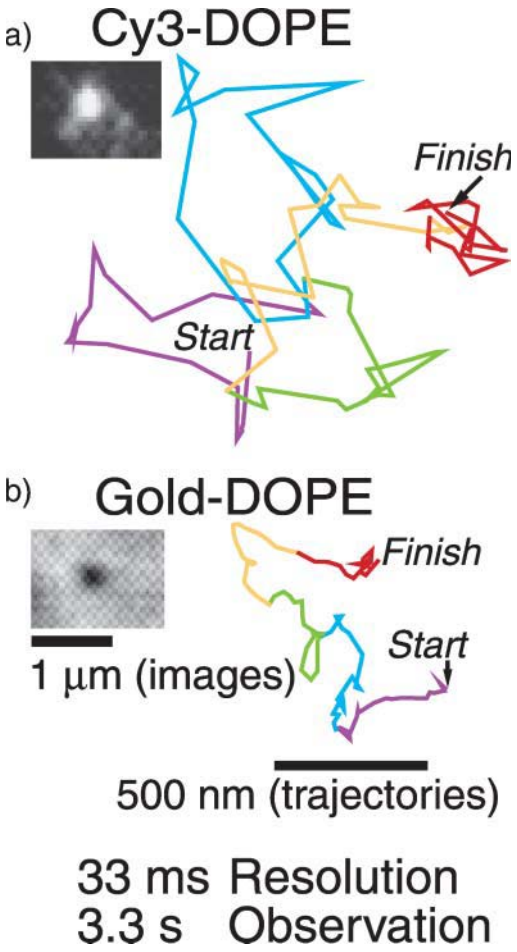

FIGURE 1 Typical images and trajectories of Cy3- and Gold-DOPE recorded at a 33-ms resolution (video rate) for 3.3 s (100 frames). (*a*) SFVI of Cy3-DOPE. (*b*) SPT of Gold-DOPE (gold probes coated with anti-fluorescein antibody Fab fragments bound to fluorescein-DOPE, which was preincorporated in the cell membrane). The colors (*purple*, *blue*, *green*, *orange*, and *red*) represent the trajectories over time periods of 20 steps (every 660 ms). The color sequence is consistent throughout this article. The actual video images are also shown.

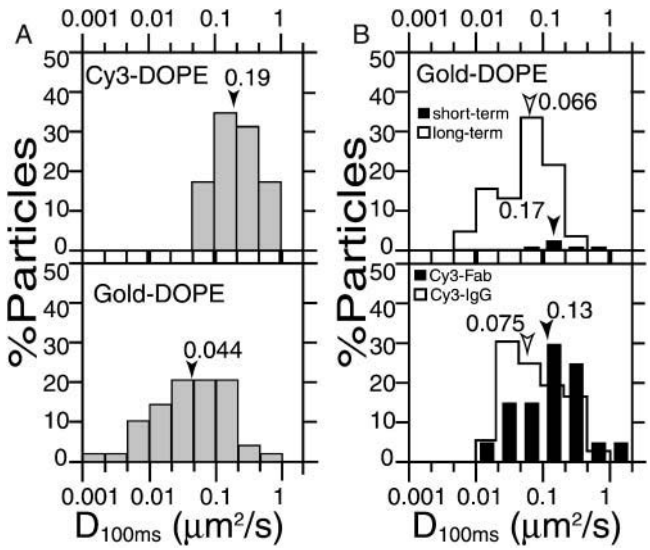

FIGURE 2 Distribution of diffusion coefficients in a 100-ms time-window (D_{100ms}). D_{100ms} is the same as D_{2-4} in Kusumi et al. (1993). Arrowheads indicate the median values. (*A*) D_{100ms} estimated for Cy3- (*top*) and Gold-DOPE observed using our standard observation protocol (*bottom*), which involves the observation of all of the gold particles attached to the membrane longer than 3 s, but the observation is limited for 20 min after the addition of the gold probes. (*B*) (*Top*) D_{100ms} for Gold-DOPE estimated for particles bound to the membrane surface for shorter periods (between 3 and 150 s, the short-term reporters, *solid bars*) and for those bound for longer periods (5 min or longer, the long-term reporters, *open bars*), indicating that those bound to the membrane for short periods exhibit diffusion coefficients comparable to Cy3-DOPE. See the text for details. Note that for the determination of the long-term reporters, we only observed for 5 min, and did not examine how much longer than 5 min they stayed on the membrane surface, whereas the observation following the standard protocol would include the short-term reporters as well as the gold probes that might have stayed much longer than 20 min, and therefore, its D_{100ms} distribution becomes broader than that for the short-term reporters and the long-term reporters combined. (*Bottom*) Fab fragments and the whole IgG of anti-fluorescein antibodies were labeled with Cy3, and their diffusion coefficients after binding to fluorescein-DOPE were measured. D_{100ms} estimated for Cy3-Fab-DOPE (*solid bars*) and Cy3-IgG-DOPE (*open bars*).

In all of the measurements using colloidal-gold probes in this research (unless otherwise stated), they were made within 20 min after the addition of gold probes: sufficient concentrations of gold particles are always present in the observation medium, and they are in dynamic equilibrium with those bound to the cell surface (standard observation protocol). Fig. 1 *b* shows a typical trajectory of a Gold-DOPE complex recorded at video rate (33-ms resolution). A statistical analysis (Kusumi et al., 1993) classified it into the simple Brownian diffusion mode. The mean values of D_{100ms} and D_{3s} were 0.044 $\mu m^2/s$ (Fig. 2 *A*, *bottom*) and 0.028 $\mu m^2/s$ (median), respectively, which were smaller by a factor of $\sim$5 than those of Cy3-DOPE. The distributions of D_{100ms} for Cy3-DOPE and Gold-DOPE are shown in Fig. 2 *A*.

These results suggest that the diffusion of Gold-DOPE may be slowed, due to steric hindrance and/or the crosslinking effect of gold probes attached to DOPE. Previously, using the same Cy3-DOPE and Gold-DOPE, Fujiwara et al. (2002) found that these probes gave the same diffusion coefficients in the NRK cell membrane, as long as the time-window for evaluating the diffusion coefficient was $<$100 ms. This was not the case in FRSK cells. This is probably due to the very small compartment size in the FRSK cell membrane (40 nm vs. 230 nm in NRK cells), as described below. These probe molecules collide with the compartment boundaries $\sim$30 times ($[230/40]^2$) more often in FRSK cells than in NRK cells, which is likely to make the D_{100ms} of Gold-DOPE very sensitive to low levels of gold-induced crosslinking of DOPE.

Evaluation of the level of crosslinking by gold probes

To evaluate the degree of crosslinking by gold probes, we initially tried to directly measure the number of fluorescein-DOPE molecules bound to the gold probe on the cell surface

by carrying out SFVI of fluorescein-DOPE. However, this turned out to be impossible due to the strong signal from the gold particle even in the absence of fluorescein-DOPE (the nature of the light scattered or emitted from the gold particle could not be determined).

To examine the relationship between the crosslinking level of fluorescein-DOPE by our gold probes (multiple binding of a gold particle to the cell membrane via several fluorescein-DOPE molecules) and the diffusion coefficient of the gold-DOPE complex, we first examined the binding duration of each gold particle on the membrane surface, and obtained the distributions of the diffusion coefficients separately for the gold particles that stayed on the membrane surface between 3 and 150 s (the short-term reporters), and for those that stayed >5 min (the long-term reporters, Fig. 2 *B*). Those that stayed <3 s were not counted because differentiating such probes from those that nonspecifically stayed near the membrane surface is difficult.

Only ~5% of the gold probes were short-term reporters, but their D_{100ms} exhibited a distribution with the median value (0.17 $\mu m^2/s$, mean = 0.23 $\mu m^2/s$; Fig. 2 *B*, *top*, *solid bars*) comparable to those for Cy3-DOPE (0.19 $\mu m^2/s$, mean = 0.27 $\mu m^2/s$; Fig. 2 *A*, *top*). This result suggests that the short-term reporters are likely bound to single molecules of DOPE. The long-term reporters exhibited diffusion coefficients (median = 0.066 $\mu m^2/s$, mean = 0.074 $\mu m^2/s$) smaller than those for the short-term reporters by a factor of 2.5–3. These results strongly indicate that the slowed diffusion of gold probes compared with that of Cy3 probes can largely be explained by the crosslinking effect of gold probes (further examination on this point is described in the text corresponding to Figs. 5–9).

How extensively did the long-term reporters crosslink fluorescein-DOPE on the cell surface? To address this question, the following experiments have been carried out. Fab fragments and the whole IgG of anti-fluorescein antibodies were labeled with Cy3, and their diffusion rates after binding to fluorescein-DOPE in the FRSK cell membrane were measured. The Fab fragment can bind to only a single molecule of fluorescein-DOPE and the whole IgG can bind to either one or two molecules of fluorescein-DOPE. We called these molecular complexes Cy3-Fab-DOPE and Cy3-IgG-DOPE, respectively.

The distributions of their D_{100ms} values are shown in Fig. 2 *B* (*bottom*). First, we compare the distribution of D_{100ms} values for Cy3-Fab-DOPE (Fig. 2 *B*, *bottom*) with that for Cy3-DOPE (Fig. 2 *A*, *top*). The median values of D_{100ms} for Cy3-Fab-DOPE and Cy3-DOPE were 0.13 and 0.19 $\mu m^2/s$, with mean values of 0.26 and 0.27 $\mu m^2/s$, respectively. Namely, the distribution is largely similar ($P = 0.095$ in the U-test of Mann-Whitney), but ~20% of Cy3-Fab-DOPE exhibited D_{100ms} smaller than any Cy3-DOPE molecules. This result suggests that some of the Cy3-Fab fragments attached to DOPE might slightly interact with surrounding molecules, increasing the drag very slightly, but that, practically, the effect of Fab-binding to the lipid headgroup on the lipid movement is negligible.

Next, we compare the histogram of D_{100ms} for Cy3-*Fab*-DOPE with that for Cy3-*IgG*-DOPE, both shown in Fig. 2 *B* (*bottom*). The average D_{100ms} for Cy3-IgG-DOPE is smaller than that for Cy3-Fab-DOPE by a factor of ≈2, with median values of 0.075 and 0.13 $\mu m^2/s$, and mean values of 0.12 and 0.26 $\mu m^2/s$, respectively. Assuming that the fraction of Cy3-IgG-DOPE exhibiting D_{100ms} is smaller than either 0.046 (based on the comparison with the distribution for Cy3-Fab-DOPE in Fig. 2 *B*, *bottom*) or 0.1 $\mu m^2/s$ (based on the comparison with the distribution for Cy3-DOPE in Fig. 2 *A*, *top*), representing those bound to two DOPE molecules, the amount of Cy3-IgG molecules bound to two molecules of DOPE can be estimated very roughly as 36 or 61%, in the respective evaluations, whereas the remaining 64 or 39% of Cy3-IgG molecules were bound to single molecules of DOPE. Given the level of approximation for such estimates, it can be said that approximately one-half ±15% of Cy3-IgG molecules were bound to either one or two molecules of DOPE.

The observation that even such a low level of clustering (mixtures of monomers and dimers) induces the twofold reduction in the diffusion coefficient on average (Fig. 2 *B*, *bottom*), itself indicates that the two-dimensional fluid continuum model for the membrane is not applicable. The Saffman-Delbrück equation that assumes the two-dimensional fluid continuum predicts that dimerization of a diffusant will have an almost negligible effect on the diffusion coefficient. Therefore, such a large reduction upon partial dimerization of the diffusant is consistent with compartmentalization of the cell membrane (also see Table 6).

Third, we compare the D_{100ms} distribution for the long-term reporters of Gold-DOPE (Fig. 2 *B*, *top*, *open bars*) with that for Cy3-IgG-DOPE (Fig. 2 *B*, *bottom*, *open bars*). The distribution for the long-term reporters overlaps with ≈80% of that for Cy3-IgG-DOPE (Fig. 2 *B*, *bottom*, *open bars*), suggesting that the majority of gold probes may bind to one or two molecules of DOPE. Comparing these two distributions, particularly at their low ends, and assuming that the fraction of the long-term reporters that exhibited D_{100ms} <0.022 $\mu m^2/s$ represents those bound to more than two DOPE molecules, we suggest that ≈20% of the long-term reporters may be bound to three or more DOPE molecules.

Fourth, finally, we compare these distributions to that for Gold-DOPE obtained following our standard observation protocol (shown in Fig. 2 *A*, *bottom*; observing all of the gold particles attached to the membrane longer than 3 s, but the observation is limited to 20 min after the addition of the gold probes, as described above. Note that for the determination of the long-term reporters in Fig. 2 *B* (*top*), we only observed for 5 min, and did not examine how much longer than 5 min they stayed on the membrane surface, whereas the observation following the standard protocol would include the short-term reporters as well as the gold probes that might have stayed much longer than 20 min, and therefore, the

D_{100ms} distribution becomes broader than that for the short-term reporters and the long-term reporters combined). Approximately 40 and 50% of the distribution of D_{100ms} for Gold-DOPE observed in our standard protocol exhibit overlaps with those for Cy3-DOPE (Fig. 2 *A*, *top*) and Cy3-Fab-DOPE (Fig. 2 *B*, *bottom*), respectively. Meanwhile, comparing this distribution obtained under standard conditions with the histograms for the long-term reporters (Fig. 2 *B*, *top*, *open bars*) and Cy3-IgG-DOPE (Fig. 2 *B*, *bottom*, *open bars*), particularly at the low ends of the distributions, and assuming that the fraction of Cy3-IgG-DOPE that exhibited D_{100ms} <0.01 or 0.022 $\mu m^2/s$ (following similar arguments as described above), we suggest that ~15–30% of Gold-DOPE in our standard protocol may be bound to three or more DOPE molecules. Taken together, under our standard conditions, Gold-DOPE may very roughly represent 40, 40, and 20% (~±10% each) of monomers, crosslinked dimers, and crosslinked oligomers greater than dimers (due to the variations of individual probes in terms of the number of active Fab molecules and their geometrical distributions on the gold surface, any theoretical prediction for such a binding is difficult to make).

This complicates the measurements of the hop parameters for DOPE diffusion using gold probes. However, although crosslinking would affect the frequency of hops across the compartment boundaries, it would not affect the measured compartment size. Therefore, in this research, we determine the macroscopic diffusion coefficient using the video rate observations of Cy3-DOPE (at this observation rate, the hop movements over compartment boundaries cannot be seen, but the rate of macroscopic diffusion over many compartments could be obtained), and the compartment size by the high-speed SPT of gold particles.

Cy3-DOPE is an intrinsically better probe in the sense that it is free from the effect of crosslinking and the probe moiety is much smaller than the gold probe, reducing the chances of nonspecific interactions with cellular structures. Nevertheless, to achieve higher time resolutions for investigating the mechanism for the ~50-fold reduction in the phospholipid diffusion rate in the cell membrane (compared with that in liposomes and reconstituted membranes), we had to use Gold-DOPE, because the poor signal/noise ratio of single Cy3-DOPE imaging hindered observations with high spatial and temporal resolutions (making direct observations of hop movements impossible). We then tried to reach a cohesive conclusion by combining the high-speed, high-resolution SPT data (the compartment size, using Gold-DOPE) with the SFVI observations (macroscopic diffusion rate, using Cy3-DOPE; see the following sections).

Gold-DOPE shows hop diffusion at 25- and 110-μs resolutions

The movement of Gold-DOPE complexes was examined at time resolutions of up to 25 μs, an enhancement by a factor of 1350 from the normal video rate (once every 33 ms). Their typical trajectories recorded at 33-ms and 110-μs resolutions are shown in Fig. 3. At a 110-μs resolution, qualitatively, all trajectories exhibited temporal confinement (Fig. 3 *b*), with occasional hops to adjacent compartments, a process we call *hop diffusion* (Kusumi et al., 1993; Sako and Kusumi, 1994; Kusumi and Sako, 1996; Tomishige et al., 1998; Fujiwara et al., 2002). Each trajectory underwent a quantitative analysis, based on the mean square displacement plotted against time (MSD-t plot), and a statistical classification into the simple Brownian diffusion mode or the hop plus confined diffusion mode, as described previously (Powles et al., 1992; Kusumi et al., 1993; Fujiwara et al., 2002; see Materials and Methods for further details).

For example, trajectories shown in Fig. 3 *b* were classified into the hop plus confined diffusion mode, and they indicate that the Gold-DOPE moved through three, four, or five apposing compartments. Individual plausible compartments were identified by software developed in our laboratory as well as by visual examination (Fujiwara et al., 2002), and are shown in color, with the black portions of the trajectories indicating the instances of hops between compartments. As shown in Table 4, 90% of the DOPE trajectories were classified into the hop plus confined diffusion mode at a 110-μs resolution, although almost all showed apparent simple Brownian diffusion at a 33-ms resolution (Fig. 3 *a*) due to averaging of the image signal over the duration of a single camera frame of 33 ms. Thus, the video rate is clearly too slow to observe temporary confinement and hop movements.

Fig. 4 shows the distributions of the compartment size (medians, 41 and 45 nm for time resolutions of 25 and 110 μs, respectively) and the residency time within each compartment (medians, 15 ms for both time resolutions) determined for each trajectory. Since the distributions of these hop parameters are virtually the same for both the 25- and 110-μs resolutions, these results indicate that experiments carried out at a 110-μs resolution are sufficient to obtain these hop parameters. Since the average residency time within a compartment is only 15 ms, video rate observations (33-ms resolution) are clearly inadequate. For example, the trajectories shown in Fig. 3 *b* are 50–100-ms long, and thus video rate observations would have generated only 2–4 points in each trajectory, which are clearly insufficient to detect hop diffusion. The compartment size found in FRSK cells (~40 nm) is smaller than that in NRK cells (230 nm) (Fujiwara et al., 2002) by a factor of ~6, or by a factor of ~30 in terms of area.

The extracellular matrix, extracellular domains of membrane proteins, and rafts are not involved in DOPE hop diffusion

Fig. 5 shows a model for the mechanisms by which the movement of DOPE on FRSK cells could be confined in 40-nm compartments.

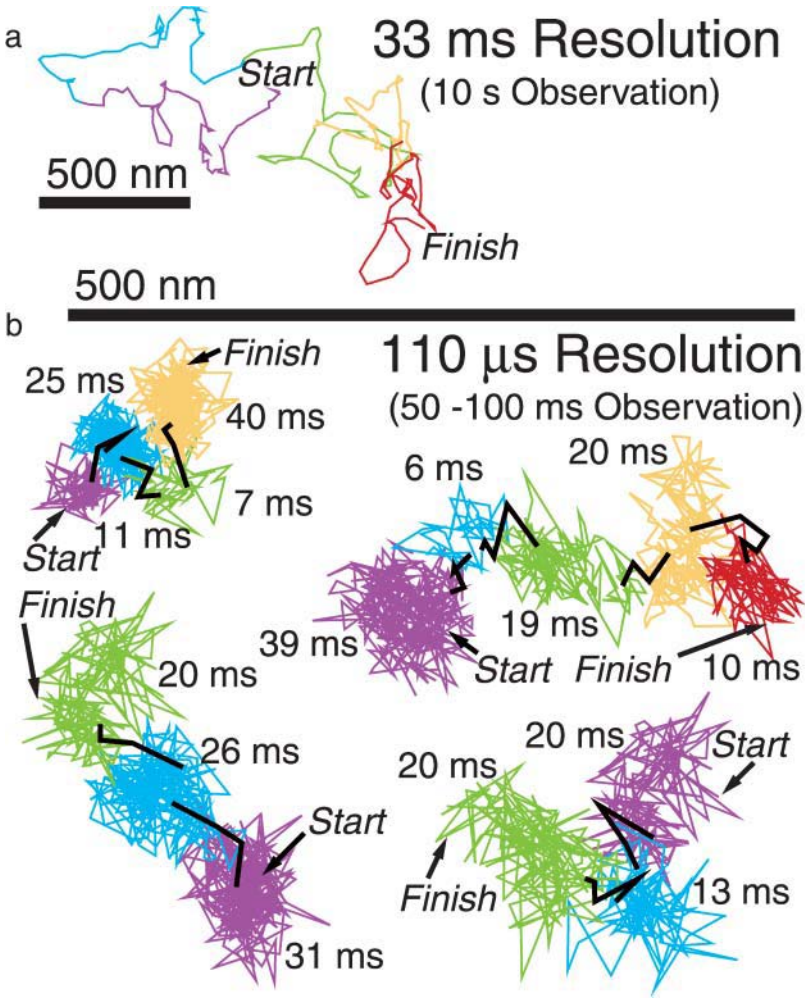

FIGURE 3 Gold-DOPE observed at a 110-μs resolution exhibited hop diffusion. What appears to be simple Brownian diffusion at a 33-ms resolution (*a*, video rate) is actually fast hop diffusion, as visible in recordings at a 110-μs resolution (*b*, 300-fold faster than the video rate). (*a*) Each color represents 60 step periods (every 2 s). (*b*) Each color indicates plausible confinement within a compartment, and black indicates intercompartmental hops. The residency time for each compartment is indicated. These compartments were detected by computer software we developed (Fujiwara et al., 2002) as well as by eye.

1. The involvement of the extracellular matrix and/or extracellular domains of membrane-associated proteins, due to interactions with Gold-DOPE.
2. Rafts acting as diffusion obstacles for unsaturated phospholipids such as DOPE, which is excluded from rafts.
3. The effect of transmembrane proteins anchored to the actin-based membrane skeleton, due to circumferential slowing effects and steric hindrance (anchored membrane-protein picket model).

We examined each model, as described below. All examinations were performed at a 110-μs resolution.

To partially remove the extracellular matrix and extracellular domains of membrane proteins, the cells were mildly treated with trypsin. To monitor the extent of the extracellular protein removal, sulfosuccinimidyl biotin was attached to the surface proteins, and was visualized by fluorescein-streptavidin (Fig. 6 *A*, *a* and *b*). A quantitative analysis of the fluorescence intensity indicated that the amount of fluorescein-streptavidin bound to the cell surface decreased to 45% after a 10 μg/ml trypsin treatment for 10 min (Fig. 6 *B*, *left*). To further examine the density of the extracellular matrix in particular, the chondroitin sulfate on the cell surface was stained by an immunofluorescence method (Fig. 6 *A*, *c* and *d*). The signal from chondroitin sulfate glycosaminoglycan decreased to 40% under the same trypsinization conditions (Fig. 6 *B*, *right*).

The movement of DOPE molecules was observed after a treatment with 10 μg/ml trypsin for 10 min (Fig. 7, *top row*, Table 5). Trypsin treatment did not affect the movement of Gold-DOPE, suggesting that the extracellular matrix proteins and extracellular domains of membrane proteins are not the main cause for the corralling of Gold-DOPE.

To determine the effects of the DOPE exclusion from rafts on its diffusion rates, we examined the consequences of partial cholesterol depletion using MβCD (Kilsdonk et al., 1995). As shown in Fig. 7 and Table 5, the temporal corralling of DOPE was not affected, suggesting that rafts are not involved in the hop diffusion of DOPE.

The actin-based membrane skeleton is responsible for cell membrane compartmentalization

To examine the effects of the actin-based membrane skeleton, cytochalasin D (final 13 μM) was added to the

TABLE 4 Parameters characterizing Gold-DOPE hop diffusion in the plasma membrane of FRSK cells observed at time resolutions of 110 μs and 25 μs

		D_{MACRO}* ($\mu m^2/s$)		Compartment size† (nm)		Residency time† (ms)		
Time resolution	Hop + confined (%)	Median	Mean ± SD	Median	Mean ± SD	Median	Mean ± SD	n‡
110 μs	92	0.042	(0.051 ± 0.041)	45	(47 ± 18)	15	(21 ± 18)	37
25 μs	89	0.035	(0.041 ± 0.032)	41	(46 ± 20)	15	(26 ± 27)	35

*Since the residency time within a compartment is 15 ms (median), D_{MACRO} represents the rate of macroscopic diffusion of molecules hopping over many compartments. The SDs include, in addition to the experimental error, the true variations in the diffusion coefficient, the compartment size, or the residency time for individual particles. The distributions for the compartment size and the residency time are given in Fig. 4. D_{MACRO} was evaluated by using 61.7-ms and 278-ms trajectories recorded at 25-μs and 110-μs time resolutions, respectively, and the MSD-t curves over 6.17 and 8.89 ms were analyzed, respectively. Since the MSD calculation involves averaging over the whole trajectory, the MSD-t curve obtained in this way contains the information of hop movements that on average take place once every 15 ms. See Materials and Methods for details.

†The compartment size was determined as $(L_xL_y)^{1/2}$, where L_x and L_y are the lengths of the confinement area in the x- and y-directions, respectively. The average residency time for each particle over a trajectory was determined as $L_xL_y/4D_{MACRO}$ for particles classified into the hop diffusion mode. The values for the residency time here are slightly different from those in Table 3 (Gold-DOPE), where the (average) residency time (averaged over all particles) was calculated from median values of D_{100ms} (median for all Gold-DOPE particles).

‡Number of observed particles.

cultured cells on the microscope stage. To obtain a cytochalasin D effect comparable to that with fibroblasts, a high concentration (increased by a factor of >10) must be used with cells of an epidermal origin, like FRSK (or *F* cells; see Kusumi et al., 1993). Observations of the DOPE movement were completed within 15 min, to observe the effect of slight actin depolymerization. Under these conditions, larger compartments appeared, with the median diameter increased by a factor of ~2, or the area by a factor of ~4, but the mode of diffusion did not change (91% hop plus confined, Table 5). Without cytochalasin D treatment, no compartments >120-nm diameter were found, whereas after the treatment, ~40% of the compartments found were >120 nm (see the *bottom left box* in Fig. 7).

Treatment with 0.5 μM jasplakinolide changed the movement of DOPE dramatically (Fig. 7 and Table 5). After the jasplakinolide treatment, approximately the same fraction of DOPE showed the hop plus confined diffusion mode (93% vs. 92%), but 40% became confined within a single compartment (no hop movement) on a timescale of 278 ms (observation time), up from 0% for total confinement without treatment. Jasplakinolide treatment increased the median residency time by a factor of 7, to 156 ms. It also increased the compartment size by a factor of 1.6. Both can be explained well by the dual effects of jasplakinolide. It first increases filamentous actin and actin bundles, with a concomitant decrease in monomeric G-actin, which then induces depolymerization of thin actin filaments, resulting in a coarser but stronger actin meshwork (Bubb et al., 2000).

The movement of DOPE molecules in membrane blebs, in which the membrane skeleton had been partially depleted, was also observed. Approximately 70% of the DOPE (as compared to ~10% in the control cell membrane) showed simple Brownian diffusion at a 110-μs resolution (Table 5).

Taken together, these results indicate that the actin-based membrane skeleton is responsible for restricting the diffusion of DOPE in untreated cells, and are consistent with the anchored-protein picket model.

The diffusion coefficient of DOPE within a small compartment is as large as that in artificial membranes

The microscopic diffusion coefficient, D_{micro}, determined by the membrane viscosity and the temperature, within the 41-nm compartments on FRSK cells, was estimated. The D_{micro}

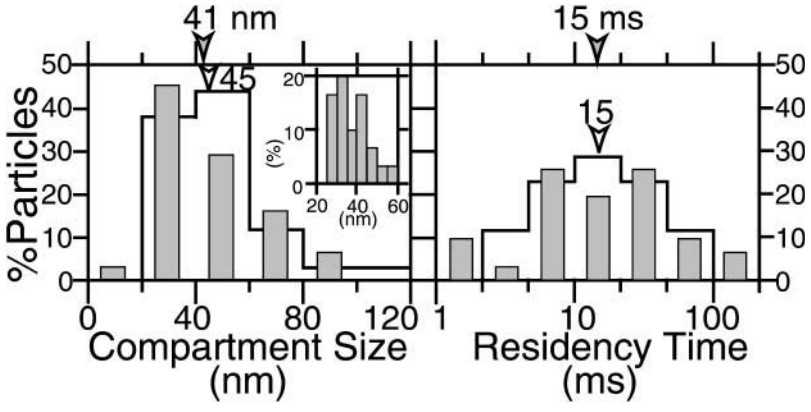

FIGURE 4 Distributions of the compartment size (*left*) and the residency time (*right*) for Gold-DOPE indicate the presence of 41-nm compartments (median observed at a 25-μs resolution) and 15-ms residency time (median) in a compartment. Open bars and solid bars indicate the distributions observed at 110-μs and 25-μs resolutions, respectively. Arrowheads indicate the median values. The inset in the histogram for the compartment size shows more detailed distributions (25-μs resolution data).

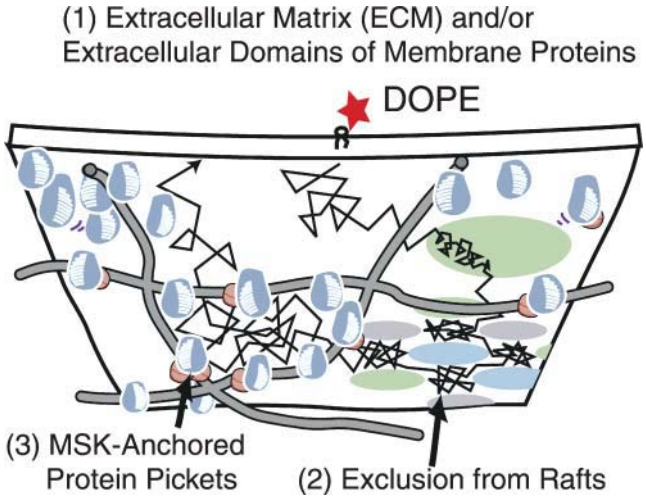

FIGURE 5 Models for the mechanisms that could be responsible for the temporal corralling and hop diffusion of DOPE.

determined for Gold-DOPE in liposomes, as well as in the bleb membranes of NRK cells after latrunculin A treatment (Fujiwara et al., 2002), over 100 μs, was $\sim$10 $\mu m^2/s$ (trajectories at least 100-μs long are needed to determine D_{2-4} or $D_{100\mu s}$ at a 25-μs resolution). If we assume that D_{micro} for DOPE in FRSK cells is also $\sim$10 $\mu m^2/s$, then the DOPE would cover an area of $\sim$60 nm across during 100 μs ($[4 \times 10\ \mu m^2/s \times 10^{-4}\ s]^{1/2}$). This is greater than the compartment size (41 nm), and therefore $D_{100\mu s}$ cannot be the correct diffusion coefficient within 41-nm compartments, but rather is an operationally defined rate, which we call the *apparent* D_{micro} here.

The relationship between the apparent D_{micro} and the compartment size, observed in control cells and bleb membranes in FRSK cells, is shown in Fig. 8 (both observed at a 25-μs resolution). The apparent D_{micro} monotonically increases with an increase in the compartment size, and asymptotically approaches $\sim 8\ \mu m^2/s$. These results indicate that the true D_{micro} in the FRSK cell membrane is likely to be comparable to that in artificial membranes or in the NRK cell membrane, suggesting that the true D_{micro} in 41-nm compartments is $\sim 8\ \mu m^2/s$.

The diffusion rate within $\sim$200-nm compartments is $\sim 5\ \mu m^2/s$, which is nearly as fast as that within 230-nm compartments in NRK cells (*the dashed blue line*). This indicates again 1), that the microscopic diffusion rate within a compartment in the cell membrane may appear small due to the lack of sufficient time resolutions (with the reduction of the compartment size, more enhanced time resolution is required); 2), that it may be basically very similar in various cell types; and 3), that the (macroscopic) diffusion in the cell membrane is reduced not because diffusion per se is slow, but because the cell membrane is compartmentalized with regard to lateral diffusion of phospholipids.

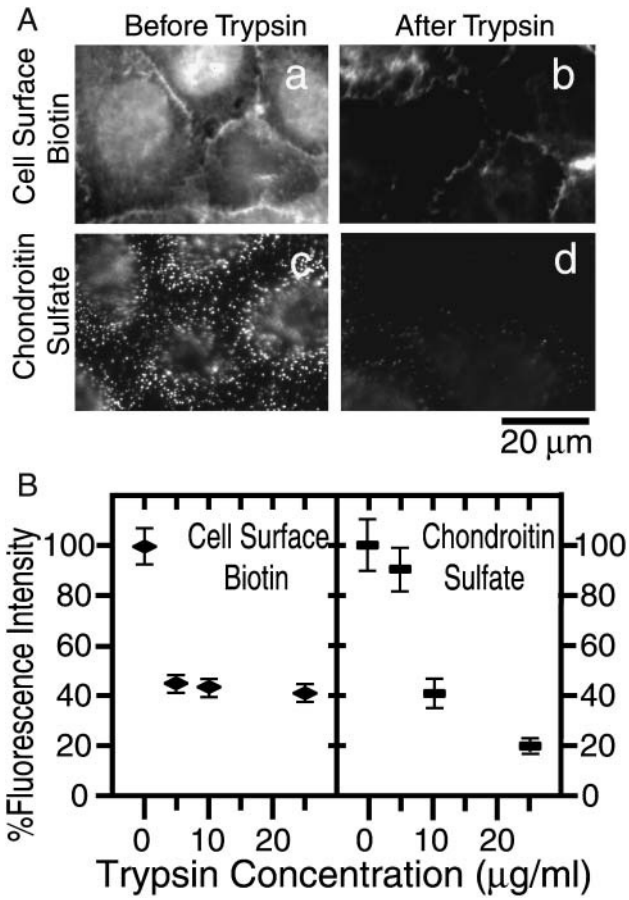

FIGURE 6 The extracellular matrices and the extracellular domains of the membrane proteins are partially cleaved by treatment of cells with trypsin. (*A*) (*a*, *b*) After the amino groups of the cell surface proteins were first tagged with biotin, the cells were incubated with 10 μg/ml trypsin (or trypsin-free medium) for 10 min and then visualized with FITC-streptavidin (biotin labeling after trypsin treatment gave nearly the same results): *a*, no treatment; *b*, after trypsin treatment. The focus of the microscope is on the lamellipodia, where most SPT experiments were carried out. (*c*, *d*) The amount of remaining chondroitin sulfate glycosaminoglycan was quantitated by immunofluorescence staining before (*c*) and after (*d*) trypsin treatment. (*B*) Fluorescence intensity due to the remaining cell surface proteins and chondroitin sulfate after trypsin treatment (10 min), plotted as a function of trypsin concentration. The fluorescence intensity (70×70 pixels $\approx 8 \times 8\ \mu m$) was normalized to that before trypsin treatment. The background was determined as the intensity in the area on the cover glass where no cell was attached, and was subtracted from the measured intensity in each area on the cell. A total of 40 cells were used for the measurements, with a total measured area of $\sim 3000\ \mu m^2$.

Compartmentalization is confirmed by quantitative anomaly analysis

To further confirm the compartmentalization of the FRSK cell membrane, we carried out a quantitative analysis using the mean square displacement (MSD), i.e., the mean *log*(*MSD*/*time*) for Gold-DOPE is plotted as a function of *log*(*time*), based on the data obtained at time resolutions of 25 μs, 110 μs, and 33 ms (Fig. 9). The slope in this display

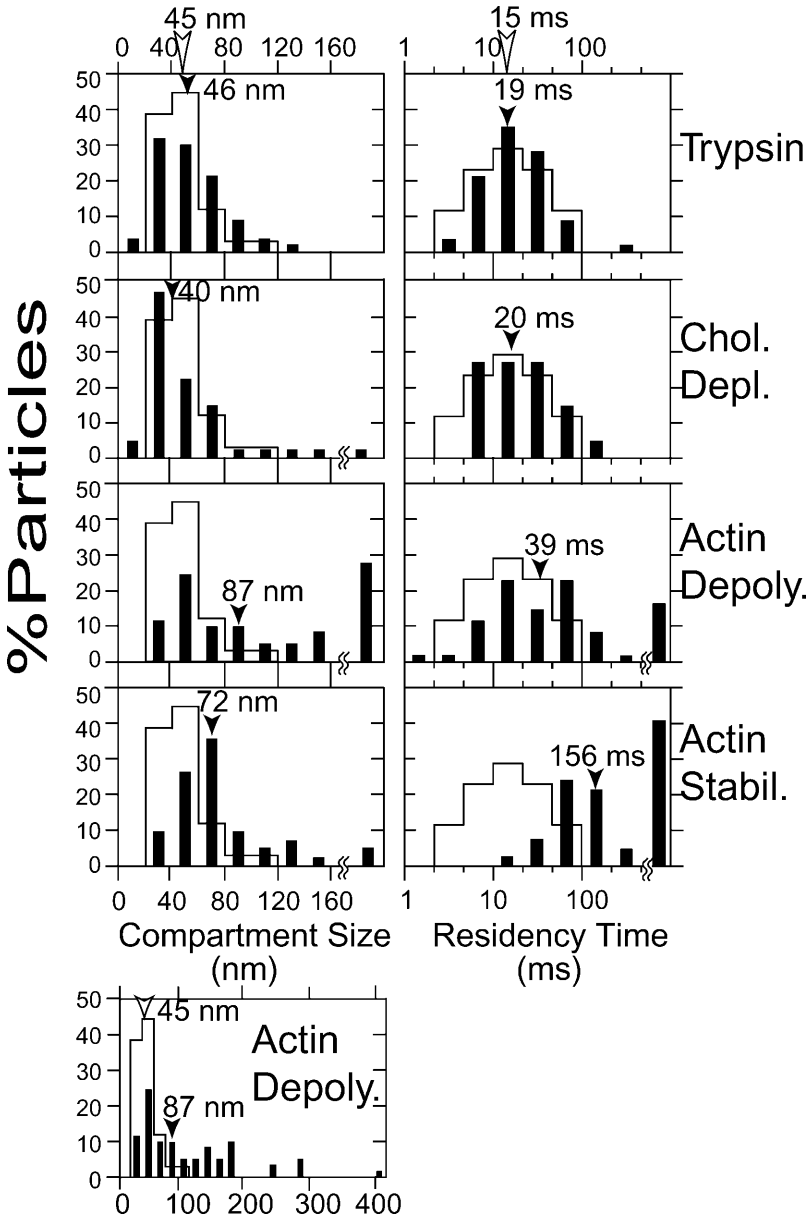

FIGURE 7 Histograms showing the distributions of the compartment size (*left*) and the residency time (*right*) after various treatments (*solid bars*). Observations were carried out at a 110-μs resolution for a period of 278 ms for each trajectory. The compartment size and the residency time were determined as described in the legend to Table 4. From top to bottom, trypsin treatment (10 μg/ml, 10 min, 68 particles), partial depletion of cholesterol by MβCD (4 mM, 20 min, 51 particles), partial depolymerization of f-actin by cytochalasin D (13 μM, 5–15 min, 68 particles), and stabilization of f-actin by jasplakinolide (0.5 μM, 5–15 min, 45 particles). In the bottom left corner, the distribution of the compartment size after cytochalasin D treatment is shown in a broader range. Arrowheads indicate median values. Open bars indicate the distributions before treatment (control, same as those in Fig. 4), and reflect the collective control results (before treatment) for all treatments.

is sensitive to diffusion anomalies. Due to the relationship $log(MSD/time) = (\alpha-1)\ log(time)$ $(0 \leq \alpha \leq 1)$, α parameterizes the level of anomaly (Saxton, 1994, 1996; Feder et al., 1996). In the case of simple Brownian diffusion, the plot becomes flat (the slope $\alpha-1 = 0$), and $\alpha = 1$ (Fujiwara et al., 2002). When diffusion is anomalous, α becomes <1, giving a negative slope ($\alpha-1 < 0$) to the plot. For DOPE molecules undergoing free Brownian diffusion in membrane blebs (Fig. 9), the plot is almost flat between 50 μs and 12 ms when observed at a 25-μs resolution. The best fit for the plot yields an $\alpha-1$ of 0.012 ($\alpha \cong 1$), which indicates that DOPE in membrane blebs undergoes simple Brownian diffusion. On the other hand, the plot for the normal cell membrane exhibits multiple negative slopes, depending on the observation time intervals. The plot can be fitted with three lines, with α-values of 0.97 (50 μs $\sim$ 0.13 ms), 0.53 (1$\sim$10 ms), and 0.94 (300 ms $\sim$ 2 s). Two transitions were found, one at $\sim$0.1 ms (or less), and the other between 10 ms and 100 ms. The former is likely to represent the collision of DOPE with compartment boundaries, and the latter is comparable to the residency times within 40-nm (15-ms) compartments. We interpret this to mean that these transitions occur at the interfaces of the following three time zones:

1. The short time zone in which Gold-DOPE corralled inside 40-nm compartments does not sense the presence of compartment boundaries (flat left end).
2. The medium time zone in which Gold-DOPE undergoes microscopic diffusion inside the compartment on short

TABLE 5 Parameters characterizing Gold-DOPE hop diffusion after treatments with trypsin, MβCD, cytochalasin D, or jasplakinolide, and those on blebs (110-μs resolution)

Treatment	Hop + confined (%)	D_{MACRO}* ($\mu m^2/s$)	Compartment size* (nm)	Residency time* (ms)	$n^\dagger$
Control	92	0.042	45	15	37
Trypsin	84	0.030	46	19	68
MβCD	80	0.028	40	20	51
Cytochalasin D	91	0.046	87	39	68
Jasplakinolide	93	0.0068	72	156	45
Bleb‡	27	0.63	180	19	36

*Median values. The distributions of the compartment size and the residency time are shown in Fig. 7.
†Number of observed particles.
‡Two types of blebs exist: those that exhibit compartment alization (27% as shown here although the compartment sizes are much greater, i.e., 180 nm median), and those that do not (73%, where Gold-DOPE exhibits simple Brownian diffusion).

timescales, although occasionally hopping to adjacent compartments (the *steep slope* in Fig. 9).

3. The long time interval in which Gold-DOPE appears to undergo simple Brownian diffusion by hopping over many compartments (*trajectories* in Figs. 1 *b* and 3 *a*, *flattened end on the right* in Fig. 9).

Although anomalous diffusion in the cell membrane could be caused by various kinds of obstacles and binding sites (Saxton, 1994, 1996), the good agreement of these transition times in Fig. 9 with the periods for free diffusion within a compartment and the residency time (15 ms) supports compartmentalization of the plasma membrane with respect to DOPE diffusion. Furthermore, the difference in these plots between intact and bleb membranes indicates the involvement of the membrane skeleton in the hop diffusion of DOPE.

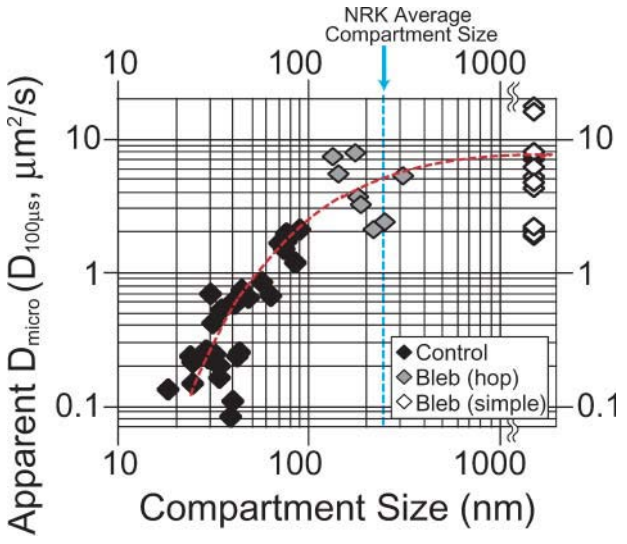

FIGURE 8 Apparent D_{micro} (in a time-window of 100 μs based on 25-μs resolution observations) plotted against compartment size, as determined for each trajectory in the control and bleb membranes. With a larger compartment size, the apparent D_{micro} increased, suggesting that in smaller compartments, even a 25-μs resolution is insufficient to obtain true diffusion rates. This figure is generated using the same data set used to generate Fig. 4 (at a 25-μs resolution, *solid bars*) and the bleb data obtained at a 25-μs resolution. The average compartment size for NRK cells is indicated (*dashed blue line*). The dashed red line is a visual aid.

Estimation of the correct hop rate

D_{100ms} and D_{3s} for Gold-DOPE are smaller by a factor of ~5 than those for Cy3-DOPE (Table 3). This difference is probably due to the crosslinking effect of gold probes, rather than the interaction of gold probes with the extracellular matrix and extracellular domains of membrane proteins, as trypsin treatment did not affect the movement of Gold-DOPE. Cy3-DOPE would give more correct macroscopic diffusion rates over many compartments, and thus a more correct hop rate, whereas the low time resolution of SFVI does not allow direct observation of the hop events and compartment size. In contrast, SPT of Gold-DOPE would provide the correct compartment size (41 nm), although it cannot give the correct hop rate because of the crosslinking of DOPE molecules, which would enhance interactions with the anchored protein pickets. Therefore, the correct hop rate can be estimated using the D_{100ms} of Cy3-DOPE (median = 0.19 $\mu m^2/s$, Table 3) and the 41-nm compartment size obtained by using Gold-DOPE, thus yielding an average of once every 2.3 ms ($[0.041\ \mu m]^2/4 \times 0.19\ \mu m^2/s$).

Monte Carlo simulations of the point diffusant in the presence of anchored-protein picket lattices

A series of Monte Carlo simulations of phospholipids diffusion, including the effects of steric hindrance and circumferential slowing caused by proteins anchored to the membrane skeleton (Sperotto and Mouritsen, 1991; Almeida et al., 1992), were carried out to examine if the anchored protein-picket model could be applicable to the case of an extremely small compartment size (41 nm on average) and a short residency time (2.3 ms). The residency time within a compartment, as determined from the Monte Carlo

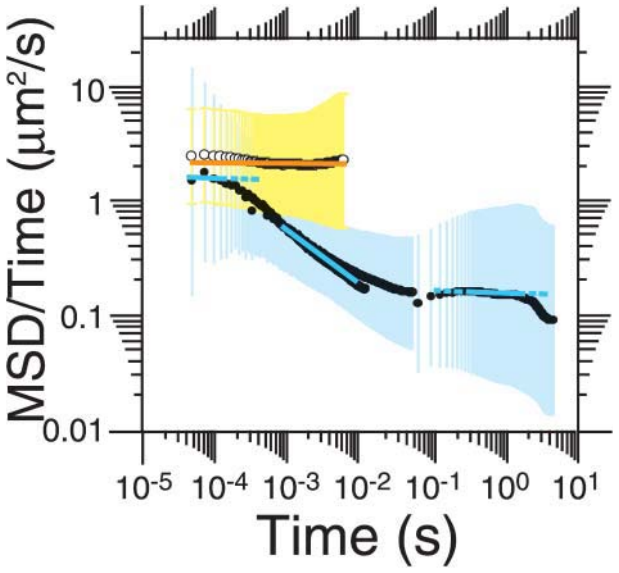

FIGURE 9 Plots of *log*(*MSD*/*time*) against *log*(*time*) provide useful information on the changes of the diffusion characteristics that depend on the observation time intervals. MSD of the trajectories was estimated using data obtained at time resolutions of 25 μs (5000 frames long), 110 μs (5000 frames long), and 33 ms (500 frames long), for the time-windows where the theoretically expected statistical errors in MSD are <40% (Qian et al., 1991). Then, the mean *log*(*MSD*/*time*) values (●) and their standard deviations (*blue* and *yellow* vertical bars, which may look like a band due to the high density of the data points here) were plotted as a function of *log*(*time*). Normal (simple Brownian) and anomalous diffusion can be distinguished in this display as lacking time-dependence (*slope* ~ 0) and having negative slopes, respectively (Saxton, 1994; Feder et al., 1996). The best fit for the data obtained for the cell membrane using the three linear segments, depicted by blue lines, with α-values of 0.97 (50 μs ~ 0.13 ms), 0.53 (1 ~ 10 ms), and 0.94 (300 ms ~ 2 s) gives transitions at ~0.1 ms (or less) and between 10 and 100 ms. (Fitted regions are shown in *solid lines*. To help the eye, they are extended, which are shown in *broken lines*. The fit between 1 and 10 ms appears bad, but in fact there are many more points in the lower black sequence of ●; i.e., the fit was done correctly.) For comparison, the plots for the trajectories in bleb membranes (○ = 1000 frames; $n = 24$) and the best regression result (*orange line*, $\alpha = \sim 1.0$) are also shown.

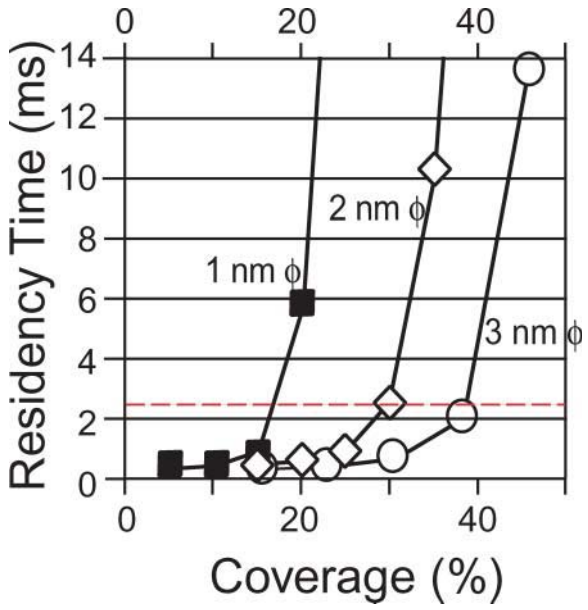

FIGURE 10 Two-dimensional, Brownian dynamics/Monte Carlo simulations indicate that ~17% coverage of the boundary with 1-nm-ϕ transmembrane anchored proteins is sufficient to reproduce the experimentally determined hop rate of 2.3 ms on average. The average residency time of Monte Carlo particles in a 40-nm compartment is plotted against percent of coverage of each side of the square compartment. The red broken line indicates the experimentally determined residency time (2.3 ms). The results indicate that seven 1-nm proteins (~17% coverage), six 2-nm proteins (~30% coverage), or five 3-nm proteins (~38% coverage), located along each side of the square compartment, were needed to reproduce the experimental residency time values of 2.3 ms.

simulations, is plotted as a function of barrier coverage, with the dashed red line showing the experimentally determined 2.3-ms residency time for 40-nm compartments (Fig. 10). Approximately 17, 30, or 38% coverage of each side of a square compartment, corresponding to seven 1-nm proteins, six 2-nm proteins, or five 3-nm proteins, respectively, were needed to reproduce the experimental residency time of 2.3 ms, supporting the anchored-protein picket model.

DOPE undergoes hop diffusion in all of the cultured cells examined

We carried out diffusion measurements for CHO, PtK2, HEK293, HeLa, HEPA-OVA, and T24 cells as well as for FRSK and NRK cells, using both SPT and SFVI. We found that in all of the eight cells examined here, DOPE undergoes hop diffusion over the compartments in the cell membrane. In Table 6, we summarize the compartment size, the residency time within a compartment, and the macroscopic diffusion rate of DOPE ($D_{100\text{ms}}$). These results suggest that the compartmentalization of the cell membrane with respect to diffusion of phospholipids is the general feature of the cell membrane in all the cells (Fig. 11).

Probability of passing a barrier when the lipid is already at the boundary varies a factor of ~7 over all of the cell types

The macroscopic diffusion rate depends on how easily a DOPE molecule at a compartment boundary can pass the barrier, i.e., the probability of passing a barrier when the membrane molecules are already at the boundary (*PP*), as well as the frequency with which a DOPE molecule reaches the compartment boundary. *PP* was determined by using the equations of Powles et al. (1992; see footnote ¶ in Table 6, this article). In this way, the value of *PP* is normalized for the compartment size; i.e., *PP* is a quantity that depends on the interaction between the barrier and the membrane molecule, as well as the properties of the barrier, but it does not depend on the compartment size. In the absence of barriers, the

TABLE 6 Compartment size, residency time, D_{100ms}, and probability of passing a single barrier for DOPE determined by SPT of Gold-DOPE and SFVI of Cy3-DOPE in the dorsal/apical membrane of various cell types

Cell type	Compartment size*† (L; nm)	Residency time‡ (τ; ms)	D_{100ms}*§ ($\mu m^2/s$)	PP¶	$\frac{PP \text{ (test cell)}}{PP \text{ (FRSK)}}$
Monomeric DOPE (Cy3-DOPE)					
FRSK	ND	2.3	0.19 (0.27 ± 0.20)	0.011	1
CHO-B1	ND	1.0	0.24 (0.30 ± 0.23)	0.019	1.6
HEPA-OVA	ND	1.5	0.21 (0.37 ± 0.43)	0.015	1.3
PtK2	ND	0.97	0.48 (0.53 ± 0.30)	0.028	2.4
HEK293	ND	3.0	0.38 (0.41 ± 0.18)	0.015	1.3
HeLa	ND	5.4	0.21 (0.31 ± 0.31)	0.0079	0.69
T24‖	ND	17	0.17 (0.22 ± 0.14)	0.0040	0.35
(NRK**	ND	410 (for 750-nm compt.)	0.34 (0.42 ± 0.13)** (D_{3s})	0.0031	0.27)
(NRK**††	[230 (240 ± 96)** ††	13	1.1 (1.2 ± 0.67)** †† (D_{50ms})	0.013	1.2])
Oligomeric DOPE (Gold-DOPE)					
FRSK	41 (46 ± 20)	9.8	0.044 (0.086 ± 0.12)	0.0026	0.23
CHO-B1	32 (42 ± 32)	4.8	0.051 (0.059 ± 0.03)	0.0040	0.35
HEPA-OVA	36 (40 ± 15)	5.2	0.061 (0.12 ± 0.16)	0.0042	0.37
PtK2	43 (44 ± 16)	1.5	0.33 (0.33 ± 0.16)	0.018	1.6
HEK293	68 (71 ± 31)	8.4	0.14 (0.14 ± 0.080)	0.0051	0.44
HeLa	68 (68 ± 27)	14	0.083 (0.10 ± 0.083)	0.0031	0.27
T24	110 (120 ± 53)	16	0.19 (0.20 ± 0.077)	0.0043	0.38
(NRK**	750 (800 ± 260)**	630 (2-ms resol.)	0.22 (0.24 ± 0.063)** (D_{3s})	0.0018	0.16)
(NRK**††	[230 (240 ± 96)**††	13	1.1 (1.2 ± 0.67)**†† (D_{50ms})	0.013	1.2])

*Median values. Mean values and standard deviations are shown in parentheses. The SDs include, in addition to the experimental error, the true variations in the diffusion coefficient or the compartment size for individual particles. The distributions for FRSK cells are shown in Figs. 2 and 4.

†The compartment size was directly obtained by SPT, carried out at time resolutions of 25 μs using Gold-DOPE. $L = (L_x L_y)^{1/2}$. Refer to the note (**) below regarding the NRK data.

‡For monomeric DOPE, the residency time was calculated using D_{100ms} (median), obtained from SFVI observations of Cy3-DOPE, and the compartment size (L, median), obtained from SPT of Gold-DOPE using the equation $\tau = L^2/4D_{100ms}$. For oligomeric DOPE, the median values obtained from SPT observations of Gold-DOPE were used. The residency time value for oligomeric DOPE on FRSK is slightly different from those in Table 4, where the (average) residency time was first obtained for individual particles. Refer to the note ** below regarding the NRK data.

§D_{100ms} values for monomeric Cy3-DOPE in FRSK, CHO-B1, HEPA-OVA, PtK2, HEK293, HeLa, and T24 cells were obtained by using SFVI. D_{100ms} values for oligomeric DOPE were obtained by using SPT of Gold-DOPE probes, which are colloidal-gold probes coated with very low amounts of Fab antibodies (see Materials and Methods), inducing low levels of crosslinking while keeping reasonable levels of specific binding. Refer to the note ** below regarding the NRK data.

¶$PP = R_D R_L/(R_D\,(2R_L{-}1) + 1)$ is the probability of passing a barrier when the membrane molecule is already at the boundary (a parameter for the diffusion in one dimension), where $R_D = D_{MACRO}/D_{micro}$ and $R_L = l/L$. l is the average distance traveled per frame, which is $= (2D_{micro}\ 25\ \mu s)^{1/2}$ (Powles et al., 1992). We assumed that D_{micro} inside a compartment in any cell membrane is 8 $\mu m^2/s$, as measured here (see Fig. 8 and related text) and by Fujiwara et al. (2002) in NRK cells, and D_{100ms} was used as D_{MACRO} (except for NRK cells, where the lipid diffusion is more complicated due to double, i.e., nested, compartmentalization). The PP values normalized against that of monomeric DOPE in the FRSK cell membrane are also shown. The effects of crosslinking were smaller in NRK, T24, and PtK2 cells as compared with those in other cells, probably due to the coupled effects of compartment size and PP (the greater these values become, the less crosslinking affects D_{MACRO}). Since the SDs for D_{100ms} (Cy3-DOPE) and L (Gold-DOPE) are in the ranges between 2/3 and 4/3 of their mean values, the SDs for the residency time and PP are probably <70% of the mean values given in this table. Note that these SDs include true variations as well as measurement errors.

‖In T24 cells, D_{100ms} was found to depend on the level of cell confluency in the culture dish. The values at ~10% confluency are given in this table because we carry out various experiments using T24 cells at ~10% confluency. At 50 and 70% confluency, the median values for D_{100ms} are 0.29 and 0.41 $\mu m^2/s$, respectively. For other cells, they were observed when they were 30–40% confluent. The mean value of D_{100ms} for T24 cells given in Table 1 was obtained at ~10% confluency. As explained in the text, since the level of oligomerization with these gold probes is low, the cells with larger mesh sizes, T24 and NRK cells with compartment sizes of 110 nm and 230 nm, respectively, exhibit only minor changes in D_{100ms} and PP upon the oligomerization by the gold probes.

**In NRK cells, since the 230-nm compartments are themselves in turn within larger 750-nm compartments (nested compartmentalization), we did the following to obtain the estimates of D_{micro} and D_{MACRO} for the two kinds of compartments. D_{micro} for the 230-nm compartment was assumed to be 8 $\mu m^2/s$ (Fig. 8), because slight oligomerization hardly affects the diffusion coefficient for freely diffusing molecules in the membrane (such as those in a compartment observed at a much higher time resolution than 25 μs; Saffman and Delbrück, 1975). D_{MACRO} for the 230-nm compartment and D_{micro} for the 750-nm compartment were estimated in 50- and 20-ms windows (= 1.1 and 1.7 $\mu m^2/s$), respectively, using Gold-DOPE. These values are consistent with each other. This way, D_{MACRO} in the 230-nm compartments is unaffected by the 750-nm barriers, and D_{micro} for the 750-nm compartment is sufficiently averaged over the 230-nm compartments. Since D_{MACRO} for 230-nm compartments is not the true long-range diffusion coefficient, the row for the 230-nm compartment is parenthesized. As the true long-range diffusion coefficient of DOPE in NRK cells, i.e., D_{MACRO} for monomeric and oligomeric DOPE, the rate at which DOPE molecules undergo macroscopic diffusion over many 750-nm compartments, the diffusion coefficients in a 3-s window using the Cy3-DOPE and Gold-DOPE data, respectively, are listed here (this time-window was selected because it is sufficiently long compared with the average residency times of 410 and 630 ms, respectively). The values for the residency time for NRK cells are slightly different from those given in Table I in Fujiwara et al. (2002), because the definition of area is different ($L_x L_y$ here, versus $(\pi/4)L_x L_y$ in Fujiwara et al.) and also because the median values, rather than the mean values (employed by Fujiwara et al., 2002), are employed for D_{MACRO} here.

††By the reasons explained in the note **, in NRK cells, D_{50ms} better represents the macroscopic diffusion rate over the 230-nm compartments than D_{100ms} (which is rather affected by the presence of the 750-nm compartments), and therefore D_{50ms} is given for both monomeric and oligomeric DOPE. However, the accuracy for D_{50ms} determination using Cy3-DOPE is low due to poor signal/noise ratio in the 50-ms window. Since, in NRK cells, in the 100-ms window, Cy3-DOPE and Gold-DOPE gave similar diffusion coefficients, as described previously (Fujiwara et al., 2002), we give the same values to the diffusion parameters for both monomeric and oligomeric DOPE to describe the hop diffusion among 230-nm compartments, obtained with Gold-DOPE.

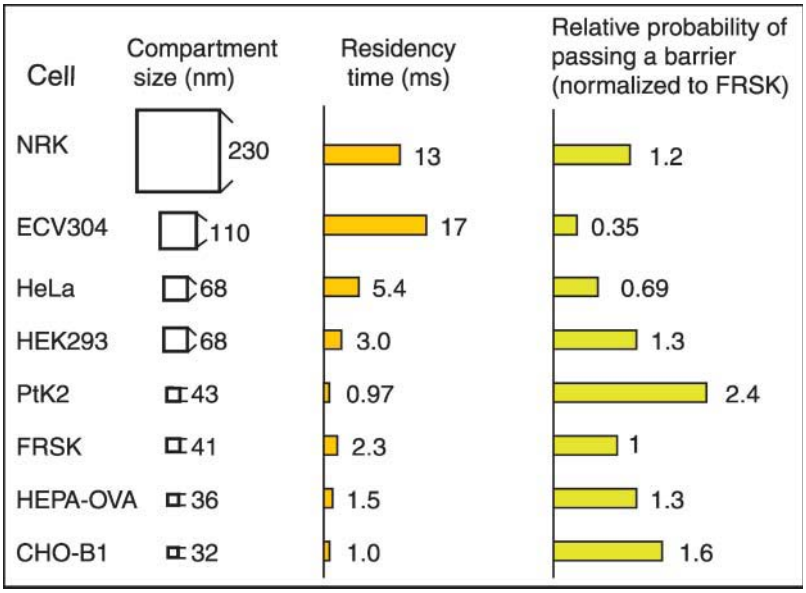

FIGURE 11 Summary of the hop diffusion parameters observed in various cell types.

DOPE molecule moves to left or right with the equal probability of $PP = 0.5$. In the presence of an impermeable barrier, the DOPE molecule never passes through the wall, and its PP is 0. In the case of a DOPE molecule always receiving the power to pass through the barriers, its PP is 1.

The overall variation in PP among various cell types is a factor of ~7 (Table 6, Fig. 11). PP would depend on the number of transmembrane proteins anchored to the membrane skeleton, the structural stability of the membrane skeleton and the membrane, and the dissociation kinetics of the actin filaments that form the membrane skeleton.

The overall variations in the residency time (a function of both PP and the compartment size) and the compartment size are factors of ~17 and ~3 (Table 6, Fig. 11), respectively (note that NRK cells are excluded from this discussion, because double compartmentalization makes the interpretation complex).

Oligomerization of DOPE greatly enhances the corralling effect

In FRSK, CHO-B1, HEK293, HeLa, HEPA-OVA, and PtK2 cells, D_{100ms} and PP for small oligomers of DOPE, induced by Fab-gold probes, were reduced by a factor of ~1.5–4 from those for the monomeric DOPE (Cy3-DOPE).

The reduction of diffusion rates upon oligomerization is at marked variance with the general understanding of the translational diffusion rate of membrane-constituent molecules in a pure lipid bilayer; translational diffusion is rather insensitive to variations in the size of the diffusing unit, if the membrane is a simple two-dimensional continuum (Saffman and Delbrück, 1975). Therefore, the results obtained with small oligomers of DOPE, as described above (Table 6), clearly show that the cell membrane cannot be regarded as a continuous fluid. It is likely that monomers hop easily from one compartment to an adjacent one, but that, upon oligomerization, the corralling effects are enhanced—greatly decreasing the hop rate, and thereby D_{MACRO}, for oligomers (Kusumi and Sako, 1996; Fujiwara et al., 2002).

Based on the SFVI observations of E-cadherin-GFP, which showed various levels of oligomerization, Iino et al. (2001) proposed that large decreases in translational mobility with the formation of oligomers can be explained by an oligomerization-induced trapping model, in which, upon oligomer formation, E-cadherin-GFP was trapped in place due to the greatly enhanced tethering and corralling effects of the membrane skeleton on oligomers. We think that the oligomerization-induced trapping model can be applied to phospholipids as well as lipid-anchored extracellular proteins, like GPI-anchored proteins. These molecules are confined by picket lines, consisting of various transmembrane proteins anchored to the actin-based membrane skeleton. When they are oligomerized by a gold particle or by liganding, they have a much lower chance of crossing a picket line, due to the increased interactions with the anchored membrane-protein pickets. Such a corralling effect would be further enhanced if liganding were to induce stable rafts (Simons and Toomre, 2000; Sheets et al., 1999).

Previously, Fujiwara et al. (2002) found that Gold-DOPE and Cy3-DOPE exhibited similar diffusion rates, as long as the time-window was kept shorter than 100 ms. Similar observations were made in this study for T24 cells (110-nm compartment size). However, since compartment sizes and residency times are much smaller in FRSK, CHO-B1, PtK2, HEPA-OVA, HEK293, and HeLa cells than in NRK cells, the effects of DOPE crosslinking were probably greater in these cells in the 100-ms window.

DISCUSSION

DOPE diffusion in the cell membrane is regulated by rows of anchored membrane-protein pickets

By employing SPT at a high time resolution and SFVI, in all of the cultured cells examined, we found that an unsaturated phospholipid diffuses macroscopically, by being temporarily confined in small compartments of 30–230 nm and then hopping among adjacent compartments once every ~1–17 ms, on average. The existence of such small domains, 30–40-nm compartments in particular, was unexpected.

Such compartmentalization depends on the actin-based membrane skeleton (although the phospholipid molecules we observed were localized in the outer leaflet of the membrane, and therefore, do not directly interact with the cytoplasmic membrane skeleton), but not on the extracellular matrix, extracellular domains of membrane proteins, or cholesterol-enriched rafts. These experimental results together with Monte Carlo simulations support the ''anchored transmembrane-protein picket model'' (Fujiwara et al., 2002). In this model, rows of transmembrane proteins anchored to the actin-based membrane skeleton act as diffusion barriers or ''pickets'', even for phospholipid molecules in the outer leaflet of the membrane, through steric hindrance and circumferential (packing and frictional) slowing.

D_{micro} (~8 $\mu m^2/s$) is very similar to that found in artificial liposomes (~5–10 $\mu m^2/s$), further indicating that macroscopic diffusion in the FRSK cell membrane is slow, not because diffusion per se is slow, but because the cell membrane is compartmentalized with regard to the lateral diffusion of unsaturated phospholipids. Since, at video rate, such small compartments cannot be detected directly, the phospholipids in the FRSK membrane may look as if they are undergoing slow, simple Brownian diffusion in a membrane with high viscosity (~40 poise, rather than 1 poise for freely diffusing lipid, using Eq. ii of Saffman and Delbrück, 1975).

Since the residency time within a compartment ranges ~1–20 ms, the diffusion coefficient strongly depends on the time-window up to ≈100 ms, but it shows only weak dependence on the time-window longer than 100 ms (Table 3, Fig. 9), which is consistent with the finding made by Vrljic et al. (2002).

Membrane compartmentalization may be a general feature of the cell membrane for all the mammalian cells

The compartmentalization of the plasma membrane and hop diffusion of lipid molecules over these compartments were found in all of the eight cells examined in this research. The compartment sizes and the residency times within the compartments vary from cell to cell, but all of the cells exhibited that their cell membranes are compartmentalized for phospholipid diffusion. Therefore, we believe that such membrane compartmentalization will be universally found, and may be a general feature of the cell membrane for all the mammalian cells. This would necessitate the paradigm shift of the way we think about the plasma membrane. We have to depart from the concept of two-dimensional fluid continuum, and should perceive the cell membrane as the compartmentalized fluid in which its constituent molecules undergo hop diffusion over these compartments. This is consistent with the observation that very low levels of crosslinking induce large reduction in the diffusion coefficient.

The viscoelastic model for the hop diffusion is not consistent with the strong dependence of the hop rate on the diffusant size

One possible model for the hop diffusion is a viscoelastic model of the complex of the fluid membrane and the elastic actin-filament meshwork, in which such hops in fact represents sudden movement of an actin filament that form the compartment boundaries. If this were to be the case, the sudden movement would affect any molecules trapped in the membrane skeleton mesh next to the moving actin filaments, and therefore, the hop rate must be the same for all the molecules, including both monomers and oligomers, irrespective of their sizes. However, in reality, the hop rate was very much dependent of the level of crosslinking (Fig. 2 *B*, Table 6). These results indicate that the viscoelastic model cannot explain the hop movement observed in this article.

Biological significance of the compartmentalization of the cell membrane

DOPE undergoes hop diffusion in all of the cultured cells examined (such as CHO, HEPA-OVA, PtK2, FRSK, HEK293, HeLa, T24, and NRK cells). We propose that the temporal confinement of lipids by transmembrane proteins anchored to the membrane skeleton is a common mechanism for reducing lipid diffusion in the cell membrane. Compartment size and hop rate vary from cell to cell, probably because of differences in the membrane-skeleton meshwork size, due to the number of proteins anchored to the membrane skeleton.

To examine the boundary characteristics in each cell, we estimated *PP*, the probability of passing a barrier, which is normalized for the size of the compartment (the microscopic diffusion coefficient within a compartment is also expected to be very similar for different cell types), and thus depends only on the dynamic interactions between the diffusant and the barrier and the intrinsic property of the boundary (such as the degree of large-scale movements of the membrane and the membrane skeleton, the on/off rate of picket proteins, and dissociation/reassociation kinetics of the actin filaments in the membrane skeleton mesh and so on). The variation of *PP* for DOPE monomers is by a factor of ~7 (~0.0040–0.028,

Table 6), indicating that the structural fluctuations of the membrane skeleton differ among different cell types. The *PP* for small phospholipid oligomers was reduced from those for monomeric phospholipids by a factor of 1–4, depending on the cell type.

''Oligomerization-induced trapping'' as already discussed in the previous sections is a consequence of both anchored-protein ''pickets'' and the membrane skeleton ''fence''. Upon the formation of signaling complexes and signaling rafts, the pickets within the membrane, as well as the fence on the cytoplasmic surface, could jointly cause the immediate arrest of such signaling complexes within or near the compartment where the extracellular signal was received (Holowka and Baird, 1996). This would allow for localization (spatial regulation) of the extracellular signal on the cell membrane.

Since the anchored membrane-protein picket barrier is effective even against the movement of individual lipid molecules in the outer leaflet, it should also be effective against GPI-anchored proteins. Therefore, oligomerization-induced trapping should play important roles in confining activated, multimerized GPI-anchored proteins and possibly the stabilized rafts formed by these GPI-anchored receptor clusters (Suzuki and Sheetz, 2001).

Another important function of the anchored-protein pickets and membrane skeleton fences may be to create the region for blocking the diffusion of membrane proteins and lipids in the otherwise fluid membrane. Nakada et al. (2003) have recently revealed the mechanism by which the diffusion barrier between the somatodendritic and axonal domains in the hippocampal neuron is generated. They found that, in the plasma membrane of the boundary region between the two domains, called the initial segment, during the development of the brain and the polarity of the neuron, various transmembrane proteins and membrane-skeletal proteins become concentrated and bound to each other, forming very dense rows of anchored-protein pickets. These create the diffusion barrier region where the macroscopic diffusion of even phospholipids is effectively blocked. Diffusion barriers have been formed in various cell membranes, including the tight junction (Dragsten et al., 1981; van Meer and Simons, 1986; van Meer et al., 1986), the neck of the bud of the budding yeast (Takizawa et al., 2000), and the boundaries between different compartments in the sperm (Ladha et al., 1997). Similar mechanisms for the formation of diffusion barriers in the cell membrane may be at work in these structures.

In conclusion, the compartmentalization of the plasma membrane is universally found and it is likely to play various biologically important roles in a variety of membrane functions.

We thank Dr. G. Marriott for providing jasplakinolide, Dr. Katrin Metz-Honda for the syntheses of Cy3-DOPE and fluorescein-DOPE, and Dr. Michael Edidin for providing HEPA-OVA cells.

REFERENCES

Almeida, P. F., W. L. Vaz, and T. E. Thompson. 1992. Lateral diffusion and percolation in two-phase, two-component lipid bilayers. Topology of the solid-phase domains in-plane and across the lipid bilayer. *Biochemistry.* 31:7198–7210.

Bubb, M. R., I. Spector, B. B. Beyer, and K. M. Fosen. 2000. Effects of jasplakinolide on the kinetics of actin polymerization. An explanation for certain in vivo observations. *J. Biol. Chem.* 275:5163–5170.

Bussell, S. J., D. L. Koch, and D. A. Hammer. 1995. Effect of hydrodynamic interactions on the diffusion of integral membrane proteins: tracer diffusion in organelle and reconstituted membranes. *Biophys. J.* 68:1828–1835.

Chang, C.-H., H. Takeuchi, T. Ito, K. Machida, and S. Ohnishi. 1981. Lateral mobility of erythrocyte membrane proteins studied by the fluorescence photobleaching recovery technique. *J. Biochem.* 90:997–1004.

De Mey, J. 1983. Colloidal-gold probes in immunocytochemistry. *In* Immunocytochemistry (Practical Applications in Pathology and Biology). J. M. Polak and S. van Noorden, editors. WRIGHT PSG, Bristol, UK. 83–112.

Dodd, T. L., D. A. Hammer, A. S. Sangani, and D. L. Koch. 1995. Numerical simulations of the effect of hydrodynamic interactions on diffusivities of integral membrane proteins. *J. Fluid Mech.* 293:147–180.

Dragsten, P. R., R. Blumenthal, and J. S. Handler. 1981. Membrane asymmetry in epithelia: is the tight junction a barrier to diffusion in the plasma membrane? *Nature.* 294:718–722.

Feder, T. J., I. Brust-Mascher, J. P. Slattery, B. Baird, and W. W. Webb. 1996. Constrained diffusion or immobile fraction on cell surfaces: a new interpretation. *Biophys. J.* 70:2767–2773.

Fujiwara, T., K. Ritchie, H. Murakoshi, K. Jacobson, and A. Kusumi. 2002. Phospholipids undergo hop diffusion in compartmentalized cell membrane. *J. Cell Biol.* 157:1071–1081.

Goldstein, J. L., S. K. Basu, and M. S. Brown. 1983. Receptor-mediated endocytosis of low-density lipoprotein in cultured cells. *Methods Enzymol.* 98:241–260.

Holowka, D., and B. Baird. 1996. Antigen-mediated IGE receptor aggregation and signaling: a window on cell surface structure and dynamics. *Annu. Rev. Biophys. Biomol. Struct.* 25:79–112.

Iino, R., I. Koyama, and A. Kusumi. 2001. Single molecule imaging of green fluorescent proteins in living cells: E-cadherin forms oligomers on the free cell surface. *Biophys. J.* 80:2667–2677.

Iino, R., and A. Kusumi. 2001. Single fluorophore dynamic imaging in living cells. *J. Fluorescence.* 11:187–195.

Kilsdonk, E. P., P. G. Yancey, G. W. Stoudt, F. W. Bangerter, W. J. Johnson, M. C. Phillips, and G. H. Rothblat. 1995. Cellular cholesterol efflux mediated by cyclodextrins. *J. Biol. Chem.* 270:17250–17256.

Koppel, D. E. 1979. Fluorescence redistribution after photobleaching. A new multipoint analysis of membrane translational dynamics. *Biophys. J.* 28:281–291.

Kusumi, A., Y. Sako, and M. Yamamoto. 1993. Confined lateral diffusion of membrane receptors as studied by single particle tracking (nanovid microscopy). Effects of calcium-induced differentiation in cultured epithelial cells. *Biophys. J.* 65:2021–2040.

Kusumi, A., and Y. Sako. 1996. Cell surface organization by the membrane skeleton. *Curr. Opin. Cell Biol.* 8:566–574.

Ladha, S., A. R. Mackie, L. J. Harvey, D. C. Clark, E. J. Lea, M. Brullemans, and H. Duclohier. 1996. Lateral diffusion in planar lipid bilayers: a fluorescence recovery after photobleaching investigation of its modulation by lipid composition, cholesterol, or alamethicin content and divalent cations. *Biophys. J.* 71:1364–1373.

Ladha, S., P. S. James, D. C. Clark, E. A. Howes, and R. Jones. 1997. Lateral mobility of plasma membrane lipids in bull spermatozoa: heterogeneity between surface domains and rigidification following cell death. *J. Cell Sci.* 110:1041–1050.

Lee, G. M., F. Zhang, A. Ishihara, C. L. McNeil, and K. Jacobson. 1993. Unconfined lateral diffusion and an estimate of pericellular matrix viscosity revealed by measuring the mobility of gold-tagged lipids. *J. Cell Biol.* 120:25–35.

Leunissen, J. L. M., and J. R. De Mey. 1989. Preparation of gold probes. *In* Immuno-Gold Labeling in Cell Biology. A. J. Verkleij and J. L. M. Leunissen, editors. CRC Press, Boca Raton, FL. 3–16.

Lindblom, G., L. B. Johansson, and G. Arvidson. 1981. Effect of cholesterol in membranes. Pulsed nuclear magnetic resonance measurements of lipid lateral diffusion. *Biochemistry.* 20:2204–2207.

Malorni, W., F. Iosi, F. Mirabelli, and G. Bellomo. 1991. Cytoskeleton as a target in menadione-induced oxidative stress in cultured mammalian cells: alterations underlying surface bleb formation. *Chem. Biol. Interact.* 80:217–236.

Miettinen, H. M., J. K. Rose, and I. Mellman. 1989. Fc receptor isoforms exhibit distinct abilities for coated pit localization as a result of cytoplasmic domain heterogeneity. *Cell.* 58:317–327.

Miettinen, H. M., K. Matter, W. Hunziker, J. K. Rose, and I. Mellman. 1992. Fc receptor endocytosis is controlled by a cytoplasmic domain determinant that actively prevents coated pit localization. *J. Cell Biol.* 116:875–888.

Nakada, C., K. Ritchie, Y. Oba, M. Nakamura, Y. Hotta, R. Iino, R. S. Kasai, K. Yamaguchi, T. Fujiwara, and A. Kusumi. 2003. Accumulation of anchored proteins forms membrane diffusion barriers during neuronal polarization. *Nat. Cell Biol.* 5:626–632.

Powles, G. J., M. J. D. Mallett, G. Rickayzen, and W. A. B. Evans. 1992. Exact analytic solutions for diffusion impeded by an infinite array of partially permeable barriers. *Proc. R. Soc. (Lond.) A.* 436:391–403.

Qian, H., M. P. Sheetz, and E. L. Elson. 1991. Single particle tracking. Analysis of diffusion and flow in two-dimensional systems. *Biophys. J.* 60:910–921.

Saffman, P. G., and M. Delbrück. 1975. Brownian motion in biological membranes. *Proc. Natl. Acad. Sci. USA.* 72:3111–3113.

Sako, Y., and A. Kusumi. 1994. Compartmentalized structure of the plasma membrane for receptor movements as revealed by a nanometer-level motion analysis. *J. Cell Biol.* 125:1251–1264.

Saxton, M. J. 1994. Anomalous diffusion due to obstacles: a Monte Carlo study. *Biophys. J.* 66:394–401.

Saxton, M. J. 1996. Anomalous diffusion due to binding: a Monte Carlo study. *Biophys. J.* 70:1250–1262.

Saxton, M. J., and K. Jacobson. 1997. Single-particle tracking: applications to membrane dynamics. *Annu. Rev. Biophys. Biomol. Struct.* 26: 373–399.

Schütz, G. J., G. Kada, V. P. Pastushenko, and H. Schindler. 2000. Properties of lipid microdomains in a muscle cell membrane visualized by single molecule microscopy. *EMBO J.* 19:892–901.

Schütz, G. J., M. Sonnleitner, P. Hinterdorfer, and H. Schindler. 2000. Single molecule microscopy of biomembranes (review). *Mol. Membr. Biol.* 17:17–29.

Sheets, E. D., D. Holowka, and B. Baird. 1999. Membrane organization in immunoglobulin E receptor signaling. *Curr. Opin. Chem. Biol.* 3:95–99.

Simons, K., and D. Toomre. 2000. Lipid rafts and signal transduction. *Nat. Rev. Mol. Cell Biol.* 1:31–39.

Smith, L. M., J. L. Rubenstein, J. W. Parce, and H. M. McConnell. 1980. Lateral diffusion of M-13 coat protein in mixtures of phosphatidylcholine and cholesterol. *Biochemistry.* 19:5907–5911.

Sonnleitner, A., G. J. Schütz, and T. Schmidt. 1999. Free Brownian motion of individual lipid molecules in biomembranes. *Biophys. J.* 77:2638–2642.

Sperotto, M. M., and O. G. Mouritsen. 1991. Monte Carlo simulation studies of lipid order parameter profiles near integral membrane proteins. *Biophys. J.* 59:261–270.

Suzuki, K., and M. P. Sheetz. 2001. Binding of cross-linked glycosylphosphatidylinositol-anchored proteins to discrete actin-associated sites and cholesterol-dependent domains. *Biophys. J.* 81:2181–2189.

Swaisgood, M., and M. Schindler. 1989. Lateral diffusion of lectin receptors in fibroblast membranes as a function of cell shape. *Exp. Cell Res.* 180:515–528.

Takizawa, P. A., J. L. DeRisi, J. E. Wilhelm, and R. D. Vale. 2000. Plasma membrane compartmentalization in yeast by messenger RNA transport and a septin diffusion barrier. *Science.* 290:341–344.

Tomishige, M., Y. Sako, and A. Kusumi. 1998. Regulation mechanism of the lateral diffusion of band 3 in erythrocyte membranes by the membrane skeleton. *J. Cell Biol.* 142:989–1000.

van Meer, G., and K. Simons. 1986. The function of tight junctions in maintaining differences in lipid composition between the apical and the basolateral cell surface domains of MDCK cells. *EMBO J.* 5:1455–1464.

van Meer, G., B. Gumbiner, and K. Simons. 1986. The tight junction does not allow lipid molecules to diffuse from one epithelial cell to the next. *Nature.* 322:639–641.

Vrljic, M., S. Y. Nishimura, S. Brasselet, W. E. Moerner, and H. M. McConnell. 2002. Translational diffusion of individual class II MHC membrane proteins in cells. *Biophys. J.* 83:2681–2692.